



Theses and Dissertations

2005-07-14

Development of a Weatherproof Windscreen for a Microphone Array

Jeffrey R. Hill
Brigham Young University - Provo

Follow this and additional works at: <https://scholarsarchive.byu.edu/etd>



Part of the [Mechanical Engineering Commons](#)

BYU ScholarsArchive Citation

Hill, Jeffrey R., "Development of a Weatherproof Windscreen for a Microphone Array" (2005). *Theses and Dissertations*. 611.

<https://scholarsarchive.byu.edu/etd/611>

This Thesis is brought to you for free and open access by BYU ScholarsArchive. It has been accepted for inclusion in Theses and Dissertations by an authorized administrator of BYU ScholarsArchive. For more information, please contact scholarsarchive@byu.edu, ellen_amatangelo@byu.edu.

DEVELOPMENT OF A WEATHERPROOF WINDSCREEN
FOR A MICROPHONE ARRAY

by

Jeffrey R. Hill

A thesis submitted to the faculty of
Brigham Young University

Master of Science

Department of Mechanical Engineering
Brigham Young University

August 2005

BRIGHAM YOUNG UNIVERSITY

GRADUATE COMMITTEE APPROVAL

of a thesis submitted by

Jeffrey R. Hill

This thesis has been read by each member of the following graduate committee and by majority vote has been found to be satisfactory.

Date

Jonathan D. Blotter, Chair

Date

Scott D. Sommerfeldt

Date

Craig C. Smith

BRIGHAM YOUNG UNIVERSITY

As chair of the candidates graduate committee, I have read the thesis of Jeffrey R. Hill in its final form and have found that (1) its format, citations, and bibliographical style are consistent and acceptable and fulfill university and department style requirements; (2) its illustrative materials including figures, tables, and charts are in place; and (3) the final manuscript is satisfactory to the graduate committee and is ready for submission to the university library.

Date

Jonathan D. Blotter
Chair, Graduate Committee

Accepted for the Department

Matthew R. Jones
Graduate Coordinator

Accepted for the College

Alan R. Parkinson
Dean, Ira A. Fulton College of Engineering and
Technology

ABSTRACT

DEVELOPMENT OF A WEATHERPROOF WINDSCREEN FOR A MICROPHONE ARRAY

Jeffrey R. Hill

Department of Mechanical Engineering

Master of Science

Microphone windscreens are typically used to reduce the noise associated with wind flowing over a microphone diaphragm by reducing the velocity of the airflow. While most windscreens are effective at reducing this noise, they do not protect the microphone from many natural elements, such as moisture, sand, and other small particles. The focus of this research was to design a windscreen that protects an array of five microphones located around a 4.5-inch diameter cylinder from these natural elements. The design goals were to have a wind noise attenuation of at least 8 dB, an insertion loss of less than 1 dB from 5-1000 Hz, and a phase shift error of less than 3% over the same range.

Computer simulations and experimental testing were used to select two basic designs. Four experimental tests consisting of wind noise attenuation, sand entrapment, insertion loss, and phase change measurements were used to optimize the geometry of

these designs. The wind noise attenuation was tested by spinning the microphone array on a long boom and by setting the array in front of a fan. Sand was blown at the windscreen in order to test how well the windscreen protects the microphone array from small particles in the velocity stream. The insertion loss of the windscreen was tested by comparing an incoming signal traveling through the windscreen to the same signal without the windscreen. Finally, the phase shift between microphones was measured using a single frequency and comparing the microphone measurements with and without the windscreen. These four tests were performed on two designs.

The first design consists of two foam filled concentric cones set around the microphone array. The second design consists of tubes that project outward from each microphone diaphragm, and then curve downwards.

Both final windscreen designs meet the desired requirements. They both reduce wind noise attenuation by approximately 9 dB in a 13 mph wind and over 16 dB in a 20 mph wind. They also have negligible insertion loss, have a phase shift error of less than 3%, and are very efficient at blocking particles from entering the windscreen.

ACKNOWLEDGEMENTS

I would like to thank all those who have assisted me in my efforts and contributed in any way to the completion of this thesis. First, I wish to acknowledge my advising professor and committee chair, Dr. Jonathan Blotter. He has dedicated many hours revising and carefully evaluating my research and writing. I also wish to thank the other two members of my committee, Dr. Scott Sommerfeldt and Dr. Craig Smith, for their helpful insights. In addition, I acknowledge help from my lab partners.

I could not have completed this work without the help and support of my wife, Jenny. Not only did she provide moral support, she proofread innumerable pages of my writing. Lastly, I recognize those moments of inspiration and thank my Father in Heaven.

TABLE OF CONTENTS

TITLE PAGE	i
SIGNATURE PAGES	ii
ABSTRACT.....	iv
ACKNOWLEDGEMENTS	vi
TABLE OF CONTENTS	vii
LIST OF FIGURES	xi
LIST OF TABLES	xv
1 INTRODUCTION.....	1
1.1 FUNDAMENTALS IN ACOUSTICS.....	1
1.1.1 Key Terms.....	1
1.1.2 Plane Waves.....	2
1.1.3 Phase Measurements.....	4
1.2 WIND NOISE.....	6
1.3 WINDSCREEN DESIGNS.....	7
1.3.1 Basket Windscreens.....	7
1.3.2 Foam Windscreens.....	8
1.3.3 Other Windscreens.....	9
1.4 PROBLEM STATEMENT.....	10
1.5 OBJECTIVE AND GOALS	10
1.6 HYPOTHESIS	11
1.7 THESIS OUTLINE.....	11
2 CFD MODELING.....	13
2.1 OVERVIEW.....	13
2.2 MODEL PREPROCESSING.....	14

2.3	MODEL ANALYSIS	14
2.3.1	Wind Noise Attenuation	15
2.3.2	Particle Entrapment.....	17
2.3.3	Insertion Loss and Phase Shift.....	19
3	EXPERIMENTAL TESTING	21
3.1	OVERVIEW.....	21
3.2	DESIGN OF EXPERIMENTS.....	22
3.3	MICROPHONE PLACEMENT	23
3.4	WIND NOISE ATTENUATION	25
3.4.1	Spinning Boom	26
3.4.2	Axial Fan.....	28
3.5	PARTICLE ENTRAPMENT TESTING	30
3.6	INSERTION LOSS TESTING	32
3.7	PHASE SHIFT TESTING.....	33
4	CONE WINDSCREEN	35
4.1	ORIGINAL CONCEPTS.....	35
4.2	BASIC GEOMETRY	36
4.3	CFD MODELING RESULTS.....	38
4.4	EXPERIMENTAL RESULTS	40
4.4.1	Factorial Designs	40
4.4.2	Wind Noise Attenuation Results.....	41
4.4.3	Particle Entrapment Testing Results.....	43
4.4.4	Insertion Loss Testing Results.....	44
4.4.5	Phase Shift Testing Results.....	45
4.5	FINAL DESIGN	46
4.5.1	Final Geometry	46
4.5.2	Final Results.....	48
5	SPIDER WINDSCREEN	53
5.1	OVERVIEW.....	53
5.2	BASIC GEOMETRY	53
5.3	CFD MODELING RESULTS.....	55
5.4	EXPERIMENTAL RESULTS.....	57

5.4.1	Wind Noise Attenuation Results.....	57
5.4.2	Particle Entrapment Testing Results.....	59
5.4.3	Insertion Loss Testing Results.....	60
5.4.4	Phase Shift Testing Results.....	61
5.5	FINAL DESIGN.....	62
5.5.1	Final Geometry.....	62
5.5.2	Final Results.....	62
6	CONCLUSIONS.....	65
6.1	FINAL DESIGNS.....	66
6.1.1	Cone Windscreen.....	66
6.1.2	Spider Windscreen.....	67
6.2	RECOMMENDATIONS FOR FURTHER RESEARCH.....	67
6.3	PUBLICATIONS.....	68
	REFERENCES.....	69
	APPENDIX.....	73
	FLUENT TUTORIAL.....	73
	Wind noise reduction.....	73
	Particle insertion.....	78
	MATLAB CODE.....	82
	M-file for wind noise testing from DAT tape.....	82
	M-file for insertion loss from DAT tape.....	84
	M-file for wind noise testing from DataPhysics.....	86
	M-file for insertion loss testing from DataPhysics.....	88
	M-file for phase shift testing from DataPhysics.....	90

LIST OF FIGURES

Figure 1-1	Transverse wave on a string.....	3
Figure 1-2	Phase difference for different pressure waves	4
Figure 1-3	Calculation of angle of incidence	5
Figure 1-4	Turbulence at microphone diaphragm	6
Figure 1-5	Wire mesh basket windscreen.....	8
Figure 1-6	Foam windscreen	9
Figure 2-1	CFD simulation of velocity reduction in a cone windscreen.....	16
Figure 2-2	CFD simulation of particles hitting a cone windscreen	18
Figure 2-3	Close up of particles entering a cone windscreen.....	18
Figure 3-1	Placement for two Larson Davis ½ inch diameter microphones	24
Figure 3-2	Placement for five PCB 1 inch diameter microphones.....	25
Figure 3-3	Boom for spinning microphone array in anechoic chamber.....	27
Figure 3-4	Mounted windscreen in anechoic chamber.....	28
Figure 3-5	Wind noise attenuation for a conical windscreen	29
Figure 3-6	Five-bladed axial fan.....	30
Figure 3-7	Sand blaster for testing windscreens in a particle flow.....	31
Figure 3-8	Sand blaster profile for testing windscreens in a particle flow	32
Figure 4-1	Original perforated cylinder concept	36
Figure 4-2	2-D side and top view of conical windscreen	37
Figure 4-3	CAD drawings of windscreen design	37
Figure 4-4	Sand insertion for Overlap = 0.5 inches, Gap = 1.5 inches	38

Figure 4-5	2-D CFD modeling of final cone windscreen	39
Figure 4-6	2-D CFD modeling of particles with final cone windscreen	40
Figure 4-7	Insertion loss of cone different foam windscreens	44
Figure 4-8	Dividers for phase change control	45
Figure 4-9	Final conical windscreen prototype	47
Figure 4-10	Wind noise attenuation for the final conical windscreen at 13 mph.....	49
Figure 4-11	Wind noise attenuation for the final conical windscreen at 13 mph (zoomed in)	50
Figure 4-12	Wind noise attenuation for the final conical windscreen at 20 mph.....	50
Figure 4-13	360° phase error plot for cone windscreen	51
Figure 4-14	Final cone windscreen geometry	52
Figure 5-1	Spider windscreen design	54
Figure 5-2	2-D view of spider windscreen variables.....	55
Figure 5-3	CFD simulations of velocity reduction in a spider windscreen	56
Figure 5-4	CFD simulation of particles hitting a spider windscreen.....	57
Figure 5-5	Wind noise attenuation for a spider windscreen.....	58
Figure 5-6	Wind noise attenuation for a spider windscreen with cloth at 20 mph.....	59
Figure 5-7	Particle testing for a spider windscreen	60
Figure 5-8	Insertion loss for a spider windscreen.....	60
Figure 5-9	360° phase error plot for a spider windscreen	61
Figure 5-10	Final spider windscreen geometry	62
Figure 6-1	Final cone windscreen geometry	66
Figure 6-2	Final spider windscreen geometry	67
Figure A-1	Scale Grid screenshot.....	73
Figure A-2	Set Units screenshot.....	74

Figure A-3	Boundary Conditions screenshot	75
Figure A-4	Velocity Inlet screenshot.....	75
Figure A-5	Solution Initialization screenshot.....	76
Figure A-6	Vectors screenshot	77
Figure A-7	Iterate screenshot	77
Figure A-8	Iterating screenshot.....	78
Figure A-9	Injections screenshot.....	79
Figure A-10	Set Injection Properties screenshot.....	80
Figure A-11	Particle Tracks screenshot.....	81

LIST OF TABLES

Table 1-1	Thesis goals.....	11
Table 4-1	First conical experiment values	41
Table 4-2	Second conical experiment values	41
Table 4-3	Wind noise attenuation factorial experiment values.....	42
Table 4-4	Sand testing factorial experiment values	43
Table 4-5	Phase difference error for cones with/without dividers	46
Table 4-6	Optimal conical configuration values	46
Table 4-7	Optimal conical final values	48
Table 4-8	Optimal conical final values	52
Table 5-1	Optimal spider final values	63
Table 6-1	Final results for cone and spider windscreen.....	65

1 INTRODUCTION

This chapter presents an overview of the theory associated with most acoustical measurements, and specifically array processing. Wind-induced noise is explained and a background of current windscreen technology is given. The objectives related to this thesis are explained, along with the specific goals for this research. The remaining chapters of this thesis are then outlined.

1.1 FUNDAMENTALS IN ACOUSTICS

There are basic principles of acoustics that are essential in the development of windscreen technology. In general, acoustics is the study of the generation, transmission, and reception of energy as vibrational waves in matter. These waves travel through air as pressure waves, and can be measured using microphones. Windscreen technology is necessary when pressure fluctuations due to wind velocity interfere with the measurement of the sound wave. Some basic terms are defined which are essential to understanding windscreen technology. When an object does not affect the sound field it is placed in, it is considered acoustically transparent.

1.1.1 Key Terms

When a pressure wave is sufficiently far from its source, the sound pressure will diminish gradually with distance. This zone is called the far field. In the far field, a

pressure wave can be considered planar,¹ because sound waves arriving from different points on the source are in phase.

A material is considered acoustically transparent if it has no effect on a sound wave passing through it. Foam is considered acoustically transparent, along with many different clothes. If a material or object is not acoustically transparent, it will create an insertion loss. Insertion loss is the measure of the pressure amplitude reduction caused by insertion of an object in the wave path. This loss is normally expressed in decibels (dB), and is calculated by differencing the measured sound pressure level with and without the object in the sound field.

Wind noise is caused when a velocity flow creates pressure fluctuations at a microphone. Wind noise attenuation is the reduction of this noise due to an object around the microphone, such as a windscreen.

1.1.2 Plane Waves

When the pressure wave is in the far field, it can be modeled like a wave on a string, as shown in Figure 1-1. The top line, t_1 represents the wave at time 1, while t_2 represents the wave at time 2. As time progresses, the wave progresses to the right.

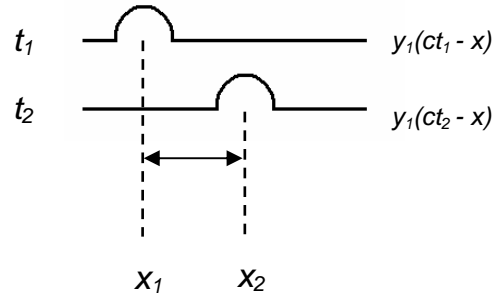


Figure 1-1 Transverse wave on a string

This wave can be described using the 1-D wave equation, Eq. (1-1). For an in-depth derivation of the 1-D equation, please see reference [1], pg. 38-40. The speed of the wave is c , y is the amplitude of the wave, t is the time, and x is the position along the string.

$$\frac{\partial^2 y}{\partial x^2} = \frac{1}{c^2} \frac{\partial^2 y}{\partial t^2} \quad (1-1)$$

Equation (1-1) is a second-order partial differential equation. Solving for $y(x,t)$, the solution contains two arbitrary functions, as shown in Eq. (1-2), where y_1 is a wave traveling in the positive direction, while y_2 is a wave traveling in the negative direction.

$$y(x,t) = y_1(ct - x) + y_2(ct + x) \quad (1-2)$$

Equation (1-2) consists of the sum of a right traveling wave, $y_1(ct - x)$, and a left traveling wave, $y_2(ct + x)$. Obviously, describing a pressure wave as planar in this way is a simplification; however, due to the location of the windscreen in the far field and the relatively small geometry of the windscreen, this work is able to take advantage of this simplification.

1.1.3 Phase Measurements

When only a 1-D wave is considered, the phase can be used to determine the direction of the wave using microphone arrays. Figure 1-2 shows a pressure wave reaching a cylinder with a five-microphone array. The distance $(x_1 - x_2)$ is the extra distance a wave must travel to reach the second microphone. As shown, when the array of microphones is rotated, the effective distance between the microphone changes.

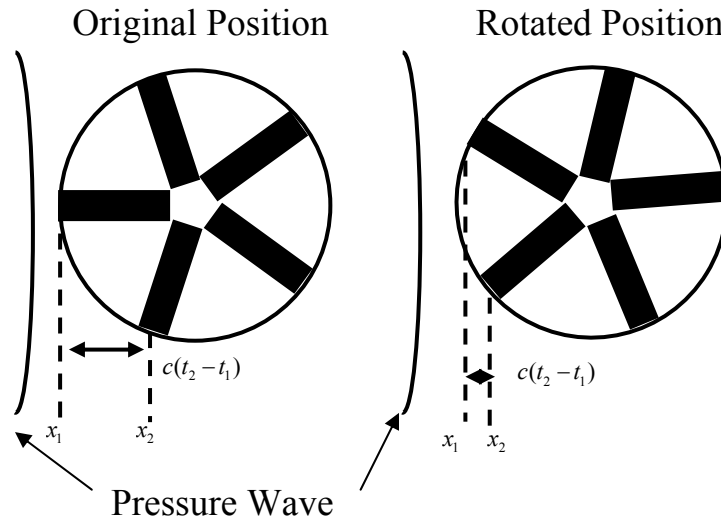


Figure 1-2 Phase difference for different pressure waves

Using Fourier transform methods, the phase of the pressure wave at each microphone can be calculated. Knowing the phase difference, $\Delta phase$, at the microphones and the frequency of the wave, f , $(x_2 - x_1)$ can be calculated using Eq. (1-3).

$$x_2 - x_1 = \Delta phase \frac{c}{2\pi f} \quad (1-3)$$

Once $x_2 - x_1$ is known, the incident angle of the pressure wave can be calculated.

First, consider a right traveling wave hitting a 5-microphone array, as in Figure 1-3.

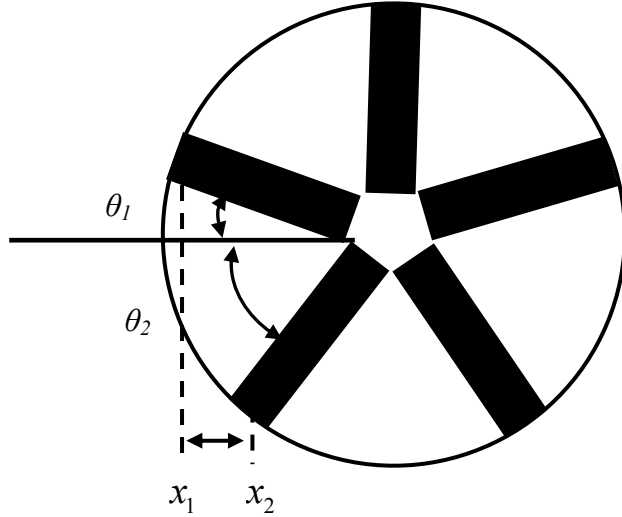


Figure 1-3 Calculation of angle of incidence

Assuming a 1-D wave, the distance between the microphones ($x_2 - x_1$) is known from the phase difference between the microphone measurements. This distance is also related to the angles between the microphones and the direction of the sound wave, as shown in Eq. (1-4), where r is the radius of the cylinder.

$$r \cos(\theta_1) - r \cos(\theta_2) = (x_2 - x_1) \quad (1-4)$$

The sum of the angles, $\theta_1 + \theta_2$ is known from the geometry, so there is only one unknown. Figure 1-3 has five symmetric microphones, so the angle between them is 72° . Equation (1-4) can be rewritten as Eq. (1-5). This equation can be solved numerically for θ_1 and the direction of the sound will be known.

$$\cos(\theta_1) - \cos(72 - \theta_1) = \frac{x_2 - x_1}{r} \quad (1-5)$$

1.2 WIND NOISE

Microphones are used to measure the acoustic pressure field in many different applications and settings. When a microphone is placed in an environment where wind is present, the ability of the microphone to measure the acoustic pressure field can be significantly degraded.

Wind typically induces noise in the microphone measurement by a combination of three processes. First, because wind is not a steady state condition, the fluctuations in the wind velocity cause low-frequency pressure fluctuations at the microphone diaphragm. Second, as the wind blows over the diaphragm and microphone casing, it creates a more turbulent flow, which also induces pressure fluctuations at the diaphragm. Third, as the wind passes around other objects, pressure waves can be created, which are then picked up by the microphone as sound.^{2,3} Figure 1-4 illustrates the first two processes where a slightly turbulent flow field is tripped to a more turbulent field as it flows over the diaphragm.

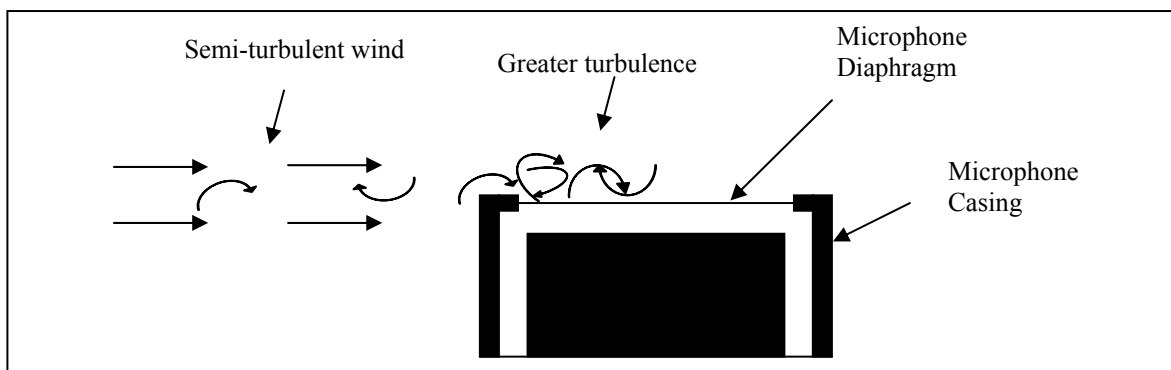


Figure 1-4 Turbulence at microphone diaphragm

1.3 WINDSCREEN DESIGNS

Although there are many different types of windscreens, they can typically be grouped as either a basket or a foam type. The objective of most windscreens is to reduce the mean flow velocity and turbulence at the microphone diaphragm.⁴ Typically, a windscreen is desired to have a small to negligible insertion loss (be acoustically transparent) while attenuating as much of the wind velocity as possible. Currently, commercial windscreens have insertion loss values of 0.1 to 0.6 dB and provide between 15 to 25 dB of wind noise attenuation at up to 30 mph.⁵ Maintaining the proper phase between each microphone is another design constraint when dealing with array windscreens. In this work it was desired to maintain a phase shift error of less than 3%.

1.3.1 Basket Windscreens

The first type of windscreen that was used is known as a basket windscreen.² It is made by completely enclosing a microphone with an acoustically transparent material, such as silk or fine-mesh cotton, which presents a large resistance to the wind.

Because the basket is larger than the microphone, it creates greater turbulence in the air than an unshielded microphone, but the turbulence is located further away from the diaphragm, thus lowering the wind noise.⁶ Most material for a basket windscreen must be supported by a frame. If the frame is large, it can interfere with the acoustic signal, but if it is small, it causes the windscreen to be fragile. Only one type of basket windscreen is commonly used, which is made by surrounding the microphone with a wire mesh, as shown in Figure 1-5.



Figure 1-5 Wire mesh basket windscreen

These wire mesh windscreens are not as effective as other basket windscreens at reducing wind noise because they are smaller and they do not add as great a resistance to the wind velocity. Larger basket windscreens made from silk or other light material are better at attenuating wind, but because of their fragility, size, and cost, they are only used when wind attenuation is paramount and cost is not an issue, such as outdoor film production.

1.3.2 Foam Windscreens

The most widely used windscreen today is made of open-celled foam, chosen because it impedes the flow of air while being acoustically transparent. Foam can either be placed directly around the diaphragm or placed so that there is an air gap between the foam and the diaphragm. An air gap will increase the attenuation of the windscreen, but requires a larger windscreen volume. One foam windscreen is shown in Figure 1-6. This windscreen has space for a small air gap between the foam and the microphone diaphragm.

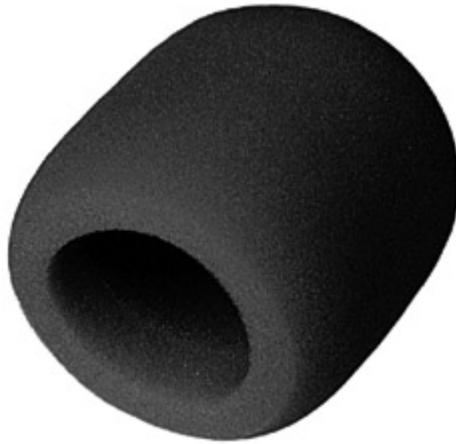


Figure 1-6 Foam windscreen

Other advantages of using a foam windscreen are that the wake caused by the windscreen is reduced,⁷ the foam does not need any external support, and the windscreen is very resilient. One disadvantage associated with foam windscreens is that the windscreen filters higher frequency signals, normally over 20 kHz.⁸ Other disadvantages are that the foam breaks down under ultraviolet light (a lifetime of less than one year under ordinary weather conditions is standard),⁹ water can clog the pores, and small particles (dirt or sand) can become trapped and drastically increase the insertion loss of the windscreen.

1.3.3 Other Windscreens

Other materials have been used to make windscreens, including fur and synthetic fibers. Fur creates very little noise as air passes through it, and it reduces wind noise very effectively.¹⁰ It is more expensive than foam, so normally it is only used when high quality measurements are needed. Additional work has been done on protecting microphones from rain by covering them with rubber¹¹ or spandex.⁴ This work has had

only limited success, because of the effect the membrane has on the frequency response of the microphone/windscreen combination.

Multi-stage windscreens are another type of windscreen used when wind noise must be reduced drastically. It combines two or more layers of windscreens in order to increase the wind attenuation. For example, a windscreen could be made of an inner core of foam, followed by an air gap, and another layer of foam or wire mesh. While multi-layer windscreens will reduce the wind-induced noise, they are more expensive, fragile, and may have a higher insertion loss than single stage windscreens.

1.4 PROBLEM STATEMENT

Current windscreen designs have focused almost exclusively on reducing wind noise and minimizing the insertion loss of the windscreen. Under short term or indoor operating conditions, these are the only two significant criteria. Under other conditions, however, additional criteria become important. For example, microphones used as tracking devices must be protected not only from the wind, but also from other natural elements, such as moisture, sand, and other small particles so the microphone is not damaged and the acoustical properties are maintained. Also, the microphone windscreens need to be constructed such that the phase between the microphones is maintained.

1.5 OBJECTIVE AND GOALS

The objective of this research is to design a windscreen that has the same basic characteristics as a commercial windscreen, while protecting an array of microphones

from the natural elements. This objective will be accomplished through the goals shown in Table 1-1.

Table 1-1 Thesis goals

1. Have a wind noise attenuation of at least 8 dB at 13 mph
2. Protect an array of five microphones from sand and dirt particles
3. Have an insertion loss of no more than 1 dB from 5 - 1000 Hz
4. Maintain the phase shift between each microphone within 3% from 5 - 1000 Hz

1.6 HYPOTHESIS

In order to achieve these goals, a number of steps will be followed for each windscreen design. Computer simulations will be developed in the computational fluid dynamics (CFD) software package, FLUENT. These simulations will create a velocity field to simulate wind around the windscreen. Particles can also be added to the simulation to act as dirt or sand. The windscreen will be placed in these simulations to understand how it will work given a variety of wind speeds and particle sizes. Using this model, the general geometry of the windscreen can be determined.

After the basic designs are chosen, they will be optimized using factorial experimental testing. Statistical analysis will be performed on the data found in these tests and an optimal design will be determined. This optimal design will be built and tested to insure compliance with the stated objective and goals.

1.7 THESIS OUTLINE

The remainder of this thesis describes the design and testing of two different microphone windscreens. Chapter 2 provides a detailed description of the computer

modeling that was performed to analyze the windscreen. Chapter 3 describes four experimental tests that were performed with each windscreen to assure that each objective is met. Chapter 4 presents the detailed results for the cone windscreen design. Both computer simulation and experimental results are given. The final optimal geometry is given, along with the results for the final design. Chapter 5 provides the results for the spider windscreen design, along with the results for the final windscreen design. Conclusions are made in Chapter 6 as well as recommendations for further research in this area. A tutorial for FLUENT and MATLAB code used to analyze the experimental data can be found in the Appendix.

2 CFD MODELING

This chapter presents in detail the model preprocessing done in Gambit and the model analysis completed in the CFD package, FLUENT. A short explanation is given on the abilities and limitations of CFD, along with how each of the four objective tests can be modeled using CFD. The four criteria tested are: 1) wind noise attenuation, 2) particle entrapment, 3) insertion loss, and 4) phase shift. The chapter is outlined as follows:

- Overview
- Model preprocessing
- Model analysis

2.1 OVERVIEW

To test multiple windscreen designs quickly, a CFD package was used. FLUENT was chosen as the CFD package because of its ability to model velocity fields, pressure fields, and free particles. Gambit was chosen as the CAD package used to import models into FLUENT. The model was built and meshed in Gambit, and then imported into FLUENT so analysis could be performed.

2.2 MODEL PREPROCESSING

Gambit is a CAD program associated with FLUENT. It has the ability to create both 2-D and 3-D models for CFD packages. Once a design is built in Gambit, it can be meshed and exported to a CFD package. In this application, some problems arise when meshing a 3-D design. The problem lies in the fact that the air around the windscreen must be meshed, not the windscreen itself. Because the gaps in the windscreen are small (between 0.25 and 0.50 inches) the mesh size must be small. However, to adequately model a steady state velocity flow over the windscreen, the overall volume of the air is substantially larger (24 to 36 inches per side). This creates a need for an extremely high number of nodes. Although this process will work, it is time consuming and computationally intense.

One way to overcome this problem is to reduce the complexity of the windscreen to a 2-D model. Once the model is meshed, it can then be exported to a CFD package for analysis. The majority of the computer modeling done in this work used 2-D models, though some 3-D models were used to assure the accuracy of the 2-D models.

2.3 MODEL ANALYSIS

To model a windscreen in a CFD package, each test must be set-up and a flow initialized. For in-depth instructions on this process in FLUENT, refer to the Appendix. The following sections explain the modeling process of wind and particle entrapment in FLUENT.

2.3.1 Wind Noise Attenuation

Wind is simulated in FLUENT by forming a velocity flow around the windscreen. By changing the velocity of the flow, the speed of the wind being modeled can be altered. For the majority of the tests performed in FLUENT, wind speeds of 35 mph were chosen. This speed is slightly higher than the wind speeds that are commercially used to test windscreens. One property of windscreens is that if the windscreen is effective at high wind speeds, it will also be effective at a low wind speed.

The results of one of the CFD models are shown in Figures 2-1. The velocity field on the outside of the windscreen is shown in Figure 2-1a. In Figure 2-1b, the outer windscreen cone is removed, so the velocity reduction at the microphones can be seen. In this example, the wind was lowered by the windscreen from 35 mph outside of the windscreen to less than 0.1 mph at the microphone surface by the windscreen.

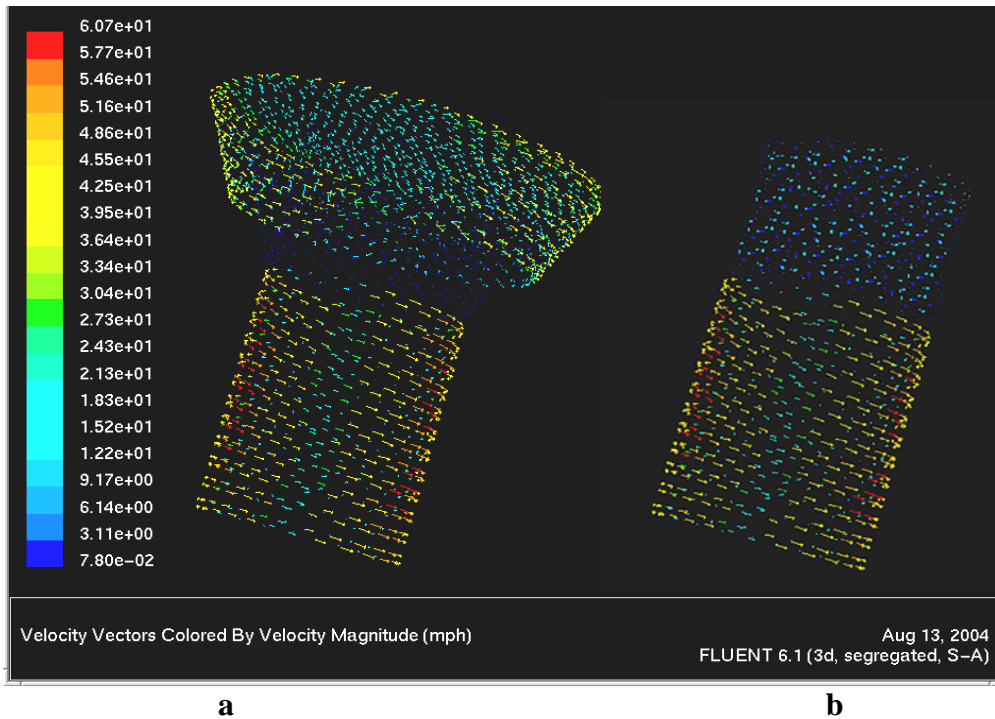


Figure 2-1 CFD simulation of velocity reduction in a cone windscreen

After initializing the flow at the given speed, multiple iterations must be performed in order for the CFD solution to converge. In most 2-D cases, the model is able to converge in fewer than 2,000 iterations, while in the 3-D cases, it can take up to 15,000 iterations before the solution converges. The default convergence criterion in FLUENT is satisfied when the error between the continuity equations at each node is less than $1.0e^{-4}$. Obviously, if the convergence criterion is slackened, it will take fewer iterations to converge. To understand the time involved, on a desktop computer with a 1.6 GHz processor and 512 MB RAM, it takes approximately five minutes per 1,000 iterations. A converged model shows the reduction of velocity at the microphone. This reduction is directly related to the wind noise attenuation because when the velocity is lowered at the microphone diaphragm, the amplitude of the pressure fluctuations caused

by the velocity flow is also greatly reduced. In this modeling process, a design was considered acceptable if there was a reduction of over 99% from the stream velocity to the velocity at the microphone.

2.3.2 Particle Entrapment

Some CFD packages, such as FLUENT, have the ability to model particles placed in the velocity flow. By varying the size and density of the particles, different materials (such as sand or dirt) can be modeled. FLUENT uses a lumped element model to simulate the airflow, and therefore will not be able to exactly model the intrinsic turbulence in the air. Because of this, FLUENT will show that either a particle will or will not enter the windscreen. Consequently, FLUENT cannot be used to predict the number of particles that will enter the windscreen, but can be used to determine the effectiveness of a specific geometric configuration.

Figure 2-2 shows particles placed in the velocity field. For each test the particles were modeled with a density of 1500 kg/m^3 and a diameter ranging from 0.0007874 to 0.079 inches in order to model sand. The flow velocity in this model was again set at 35 mph.

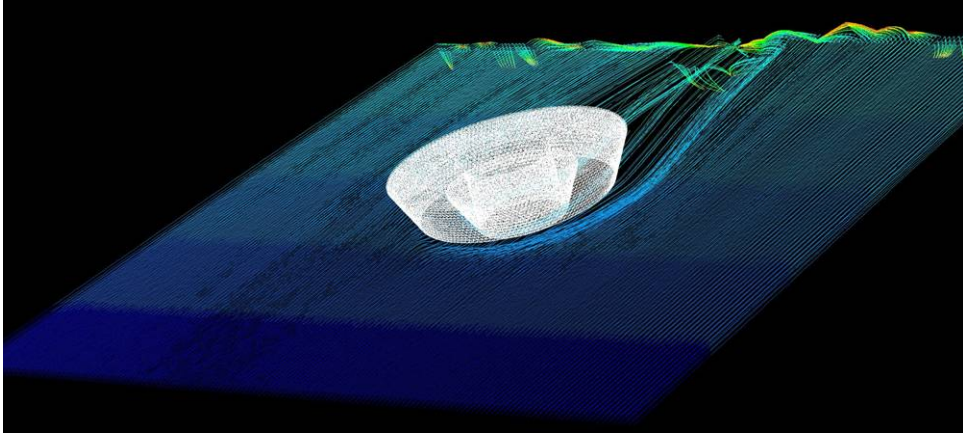


Figure 2-2 CFD simulation of particles hitting a cone windscreen

Figure 2-3 is a close-up of the same windscreen, though the outer cone is hidden so that the inside can be seen. In this model, some of the particles are shown entering the windscreen, where they become trapped. Although they don't actually reach the cylinder where the microphones are located, in these tests any particles that enter the windscreen are considered unacceptable.

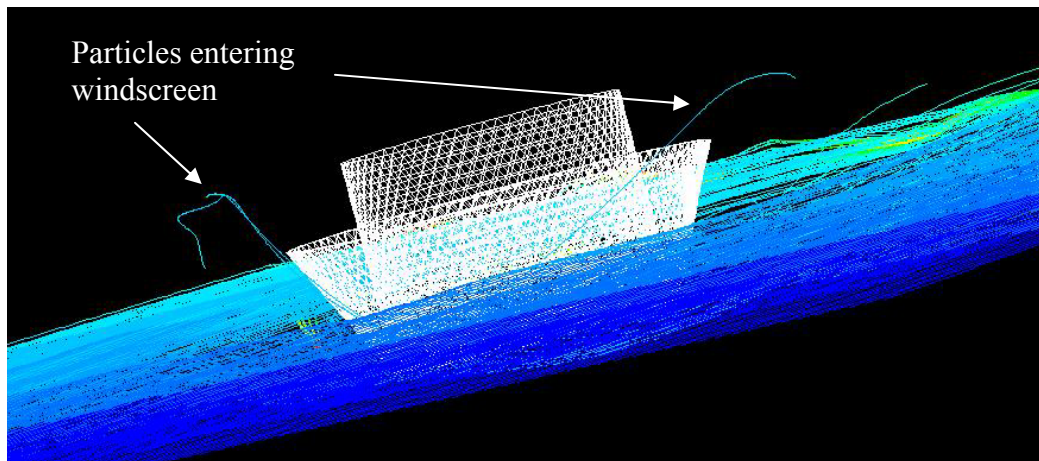


Figure 2-3 Close up of particles entering a cone windscreen

2.3.3 Insertion Loss and Phase Shift

As noted previously, each windscreen must reduce wind noise, prevent sand from entering the windscreen, have negligible insertion loss, and not alter the phase of the sound. While the first two can be modeled fairly quickly, the later two require much more time and effort to model. In order to test the insertion loss of a windscreen, a pressure wave must be created and sent through the model to determine if there is any pressure drop at the microphone. To model the pressure wave, a non-steady flow must be used, which requires at least 2000 iterations per time step to converge. In addition, the time step must be small to insure accurate results. This causes the number of iterations needed for convergence to be on the order of a hundred thousand iterations. As stated previously it takes a 1.6 GHz desktop computer 5 minutes per 1000 iterations; therefore, it would take over 8 hours of processing time to model the pressure in FLUENT. A CFD package could be used if required, but should only be done if a high cost of experimental testing makes it necessary.

3 EXPERIMENTAL TESTING

This chapter outlines the experimental testing that was performed on the microphone windscreens. A brief background of the design of experiments is given, which explains the use of factorial experiments. Each test that was performed is explained and the experimental setup is given. The chapter is outlined as follows:

- Overview
- Design of experiments
- Microphone placement
- Wind noise attenuation
- Particle entrapment testing
- Insertion loss testing
- Phase shift testing

3.1 OVERVIEW

Experimental testing has been used to analyze how different windscreen prototypes affect the measurements of the covered microphones. To test the effect of changing the geometry of the windscreen, factorial testing was used. Each objective to be tested had its own testing apparatus. Random experimental error was minimized by performing all runs of a given experiment close together, to eliminate the effect of outside variables changing over time. In addition, each time a comparison was used, both

runs were performed at the same time. Also, care was taken to insure that each experiment was performed the same way each time to insure the results were consistent. Finally, runs were randomized to lower any effects from short-term experimental error.

3.2 DESIGN OF EXPERIMENTS

A factorial experiment is able to predict optimal values for each variable in a system, while reducing the number of tests that must be performed.¹² For a factorial experiment, three values of each variable are used; a high, a low, and a center value. Each variable is tested at a high and low value which produces 2^k runs (k = number of variables). Experiments at the center point of each variable are performed to find any curvature in the model. Using statistical equations, each variable is rated for its effect on the overall system. Some variables can be statistically insignificant and can be ignored, while other variables will have a great impact on the final result. A factorial experiment is used to find the significant variables and optimize them.

To determine if a variable is statistically significant, its effect must first be calculated. The effect is calculated using Eq. (3-1).

$$effect = \bar{Y}_+ - \bar{Y}_- \quad (3-1)$$

In Eq. (3-1), \bar{Y}_+ is the summation of the responses when the variable is at its high value, regardless of the values of the other variables. \bar{Y}_- is the summation of the responses when the variable is at its low value. Once the *effect* is known, the pooled variance (s_p^2) can be determined using Eq. (3-2).

$$s_p^2 = \frac{(n_A - 1)s_A^2 + \dots + (n_N - 1)s_N^2}{n_A + \dots + n_N - 2} \quad (3-2)$$

In Eq. (3-2), N is the total number of designs, n_A is the number of repetitions for design A , and s_A is the standard deviation of those repetitions. Using the pooled variance, the standard error, s_E , is calculated using Eq. (3-3). In this equation, n_F is the total number of windscreens tested.

$$s_E = \sqrt{\frac{4s_p^2}{n_F}} \quad (3-3)$$

The t-statistic is then calculated using Eq. (3-4), which is compared to the student-t distribution, t_{crit} . t_{crit} is based on the desired confidence interval and number of repetitions.

$$t_E = \text{effect} / s_E \quad (3-4)$$

If $t_E \geq t_{crit}$, then the variable of interest is significant. For further discussion on this subject, please see reference [12].

3.3 MICROPHONE PLACEMENT

For most of the experiments, two Larson Davis microphones mounted in a 4.5-inch diameter cylinder to simulate the microphone array configuration were used. The microphones were comprised of half-inch prepolarized FF microphone, model 2551, and PRM426 ICP preamplifiers. Although each microphone was only half an inch long, the preamplifier was approximately 3.5 inches long. This required that each microphone be offset by at least a half inch up or down, as shown in Figure 3-1. For this reason and due to the size of the cylinder, only two microphones were used, placed perpendicular to each other, for most measurements.



Figure 3-1 Placement for two Larson Davis ½ inch diameter microphones

Once the final prototype windscreen was designed, new 1 inch diameter microphones (Model 377M03) were made available by PCB PIEZOTRONICS. These microphones were designed specifically for this application, and are only 1 inch deep, including the preamplifier. This allows all five to be set in the cylinder at 72° increments, as shown in Figure 3-2. As shown, all five microphones will fit without interference, and without the need to offset the microphones. With the five microphones in place, the final phase measurements were taken, along with the 360° phase plot that is shown in section 4.5.



Figure 3-2 Placement for five PCB 1 inch diameter microphones

3.4 WIND NOISE ATTENUATION

Wind noise attenuation is measured by comparing the noise generated by the wind with and without a windscreen. The wind noise attenuation is simply the average difference between the two measured over a given frequency range. In this research, the average sound pressure level (in dB) was measured over a frequency range of 0 - 100 Hz. This range of frequencies was chosen because on average, 95% of the energy of wind induced noise is located below 30 Hz,¹³ therefore, 0-100 Hz will capture most, if not all of the wind energy. Testing was done in the anechoic chamber located in the Eyring Science Center at BYU in order to reduce the noise floor of the measurement. The chamber is anechoic down to approximately 50 Hz. Unfortunately, the chamber is located near fans that provided air to the entire building. The base frequency of these fans is approximately 7 Hz, with harmonics at multiples of 7 Hz. When the fans were running, the sound floor began to infringe on the wind noise at very low frequencies.

Therefore, some of the data are only accurate for slightly higher frequencies, between 22 and 100 Hz. However, even with this complication, accurate measurements of the wind noise attenuation were possible.

To assure that the new windscreen is as effective as current foam windscreens, multiple foams were also tested for their wind noise attenuation. These wind noise attenuations were then compared to those of the new windscreen.

To generate the wind, two different methods were utilized. First, the microphone array was spun using a large boom and data were taken using a DAT tape to capture the data, which were then post-processed using MATLAB. Second, a fan was placed in front of the array to generate a wind. When using a fan, DataPhysics software was used to acquire the data, and the data were again post-processed using MATLAB. The full MATLAB code used is located in the Appendix. The code averages the wind noise attenuation from 0-30 Hz and from 0-100 Hz. The maximum attenuation over those ranges is calculated, along with the minimum attenuation and the standard deviation of the attenuation over the same frequencies. These four results were calculated in order to ensure that the wind noise was reduced over the entire frequency range, rather than only over a small range of frequencies.

3.4.1 Spinning Boom

In order to quietly generate “wind”, the microphone array was placed on a spinning arm, thus generating a velocity difference at the microphone. The apparatus for this test was mounted in the anechoic chamber, as shown in Figure 3-3. The apparatus consists of a mounted motor with a five-foot boom attached. The boom was made from $\frac{3}{4}$ inch steel tubing. The microphone cylinder was mounted 38 inches from the center of

rotation. The counterbalance weights were mounted only 22 inches from the center of rotation so as to keep the counterbalance weights from interfering with the airflow around the microphone cylinder. A Michigan Scientific S6 slip ring was used to connect the microphone outputs to the data acquisition hardware. In this set-up, two microphones were positioned with one facing the wind, and the other perpendicular, facing outward. This system was able to quietly generate winds up to 13 mph.

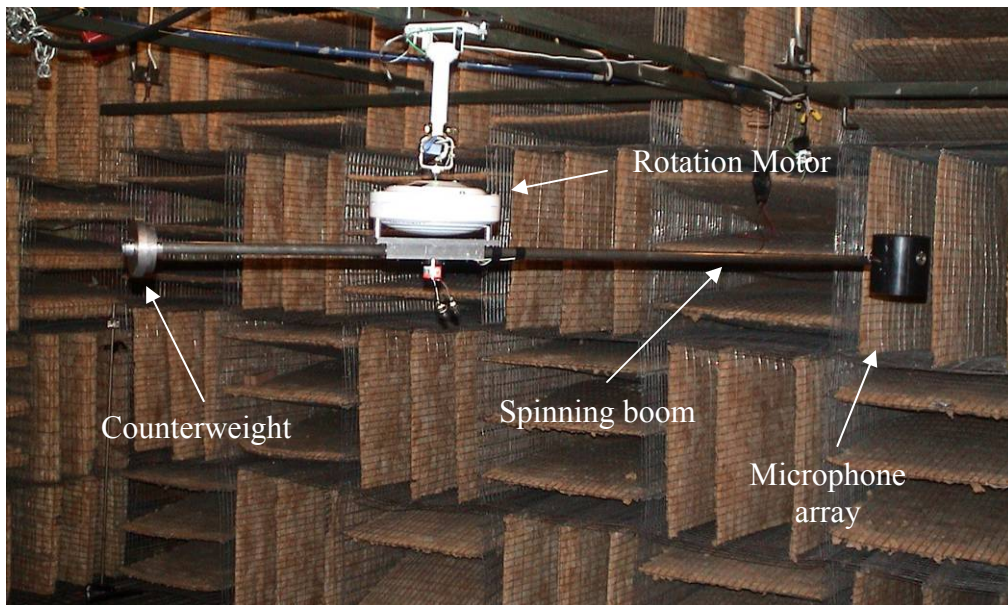


Figure 3-3 Boom for spinning microphone array in anechoic chamber

Figure 3-4 shows a close-up of one of the factorial designs mounted in the anechoic chamber at the end of the boom. Before each test, the rotating arm was counterbalanced in order to assure stability of the system.



Figure 3-4 Mounted windscreen in anechoic chamber

3.4.2 Axial Fan

Because of the increase in weight when using five microphones instead of two, it was impossible to spin the windscreen fast enough to get useful measurements. Instead, to test the wind noise attenuation, the windscreen was placed in front of an axial fan located in the anechoic chamber. Two axial fans were used. The first, a four-bladed, 115 V, 2.1 amp fan, was slightly quieter than the second fan but could only reach wind speeds up to 13 mph. Figure 3-5 is an example of data taken using the first axial fan. At 13 mph, the dominant fan frequencies can be seen at 35, 53, and 60 Hz, but they do not interfere with the wind noise attenuation measurements.

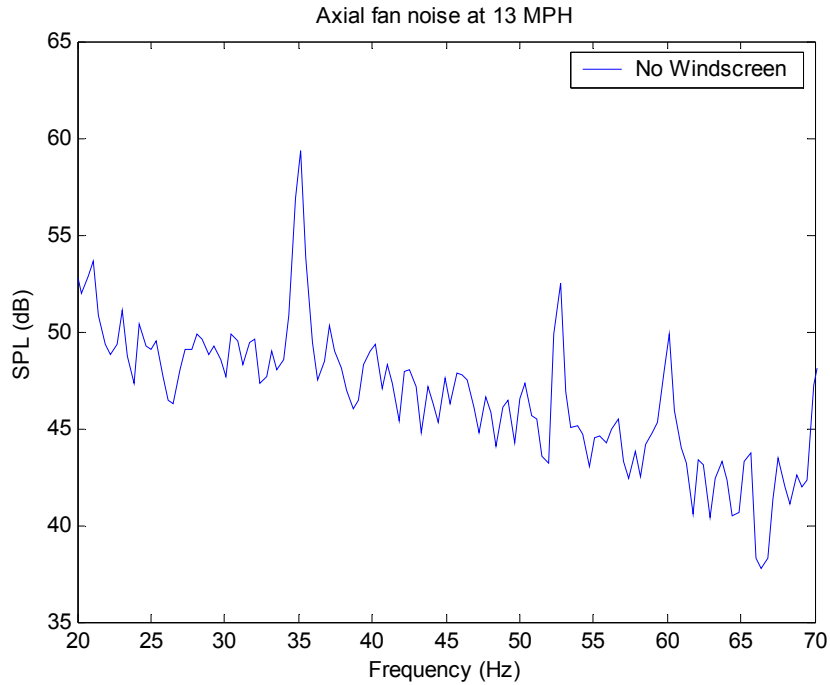


Figure 3-5 Wind noise attenuation for a conical windscreen

The second fan was able to reach wind speeds of 20 mph. This wind speed was measured with a handheld anemometer. It was an EBM W16180 five-bladed, 48 V, 100 watt fan. This fan is shown with the windscreen in Figure 3-6. This fan does not have as many dominant frequencies as the first fan, but does produce more broadband noise at low frequencies.



Figure 3-6 Five-bladed axial fan

3.5 PARTICLE ENTRAPMENT TESTING

One of the primary reasons for this research is to design a windscreen that will protect an array of microphones from sand particles in the air. In order to test the effectiveness of the windscreen, an experimental test was designed and built that allowed for the insertion of sand and dirt into a stream of high-velocity air, as shown in Figure 3-7. After a predetermined time, the amount of sand that entered the windscreen was measured.

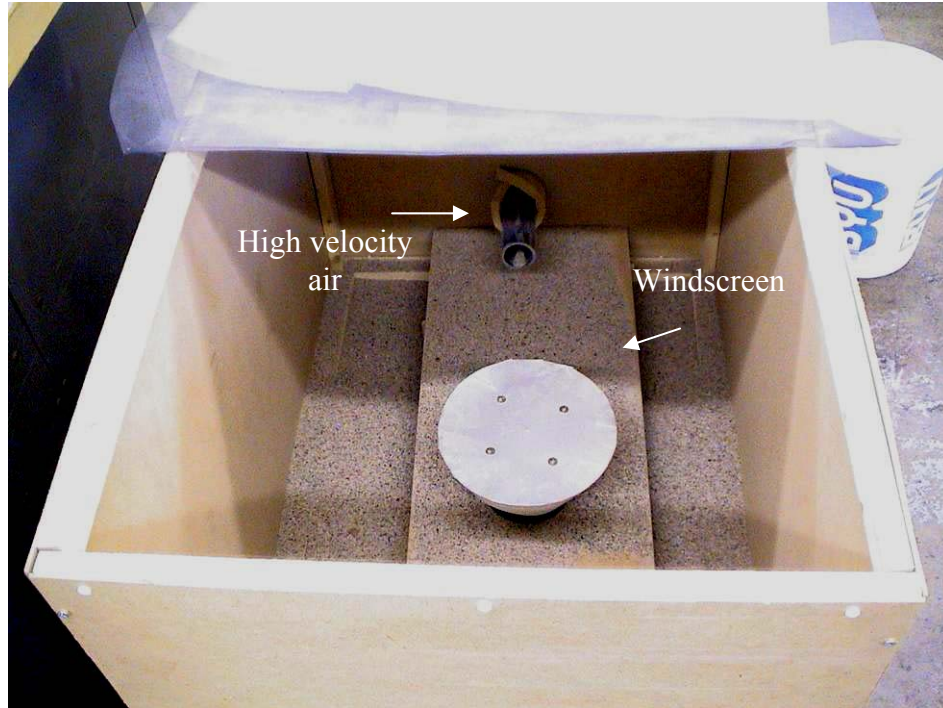


Figure 3-7 Sand blaster for testing windscreens in a particle flow

A 2 foot by 2 foot by 3 foot box was constructed from wood, with an open top. During testing, the top was covered by foam to minimize the amount of sand and dust that escaped from the box. The sand was poured into a funnel, shown in Figure 3-8, which was inserted into the air stream.

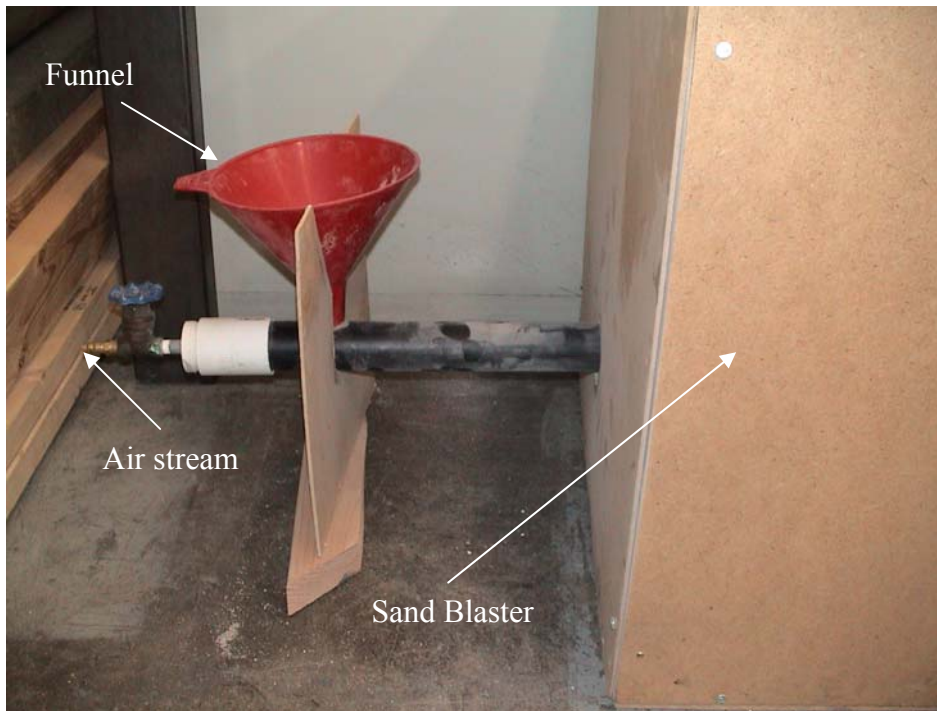


Figure 3-8 Sand blaster profile for testing windcreens in a particle flow

Using this equipment, an experiment was set up such that sand particles were inserted into the stream of high velocity air (approximately 50 mph) for 4 minutes. The amount of sand that entered the windscreen was measured by weighing the windscreen on a scale with a precision of 0.1 grams before and after sand was blown. The difference between the two measurements was the amount of sand that entered and remained in the windscreen. Optimally, there would not be any sand present in the windscreen after the test.

3.6 INSERTION LOSS TESTING

The insertion loss was tested by placing the microphone cylinder in the anechoic chamber, and producing a known output from a Mackie speaker located sufficiently far away for the microphones to be in the far field. The amplitude of the output was

measured at the microphone with the windscreen and was compared to the amplitude measured at the microphone without a windscreen. A function generator was used to produce the noise, sending a 2 volt peak-to-peak sine wave to the speaker. This was done for frequencies ranging from 50 to 10,000 Hz. As mentioned previously, the microphone cylinder was rotated, and the insertion loss was tested for each rotation. This insured that the location on the cylinder did not increase the insertion loss at a given microphone.

3.7 PHASE SHIFT TESTING

To determine the phase change caused by the windscreen, the apparatus used for insertion loss testing was utilized. For the windscreens used in the factorial testing, two microphones were located inside the cylinder, and both were recorded simultaneously as a known input was played over the source speaker. The phase of the signal measured by each microphone was calculated by performing a FFT on the data and then computing the inverse tangent of the imaginary component over the real component. The percent error between the microphone signals with and without a windscreen was computed using Equation (3-5), where M_1 is the phase (in degrees) of the signal at the first microphone in the cylinder and M_2 is the phase (in degrees) at the second microphone in the cylinder.

$$\%Error = \frac{(M_1 - M_2)_{ws} - (M_1 - M_2)_{nws}}{Phase_T} \quad (3-5)$$

In this equation, the windscreen-covered array is denoted by the subscript ws , while the non windscreen-covered array is denoted by the subscript nws . The percent error between the microphone signals was normalized using $Phase_T$, the theoretical phase difference that would be measured over the entire cylinder. This theoretical phase was

determined using Equation (3-6), where D is the diameter of the array, f is the frequency of the signal, and c is the speed of sound.

$$Phase_T = \frac{360^\circ \cdot D \cdot f}{c} \quad (3-6)$$

The final windscreen designs were tested with five microphones and used the average cross-spectrum of 10 data sets. The five-microphone array was rotated through a 70° range with measurements taken every 10° . This procedure provides measurements for the full 360° around the windscreen. The difference between each 10° increment was compared with and without the windscreen, as seen in Equation (3-7).

$$\%Error = \frac{(M_{n,p+10} - M_{n,p})_{ws} - (M_{n,p+10} - M_{n,p})_{nws}}{Phase_T} \quad (3-7)$$

In this equation, $M_{n,p}$ is the signal at microphone n and angle p , where p varies from 0° to 70° . Again, the windscreen-covered array is denoted by the subscript ws , while the non windscreen-covered array is denoted by the subscript nws . The error was again normalized using $Phase_T$, the theoretical phase difference over the entire array of microphones.

4 CONE WINDSCREEN

In this chapter, the cone windscreen design is explained. First, some of the original concepts are stated. The basic geometry of the cone windscreen is explained in detail. The remainder of this chapter will focus on analytical and experimental results.

Topics are addressed in this chapter as follows:

- Original concepts
- Basic geometry
- CFD modeling results
- Experimental results
- Final design

4.1 ORIGINAL CONCEPTS

The current windscreen in use is made by covering the microphone array with 1.5 inches of foam. One idea was to simply cover the foam windscreen with a weatherproof material that would protect the foam from any particles in the air. Unfortunately, when the foam was covered, the phase shift around the microphones was substantially altered. A second preliminary concept was to surround the microphones with perforated cylinders as shown in Figure 4-1.

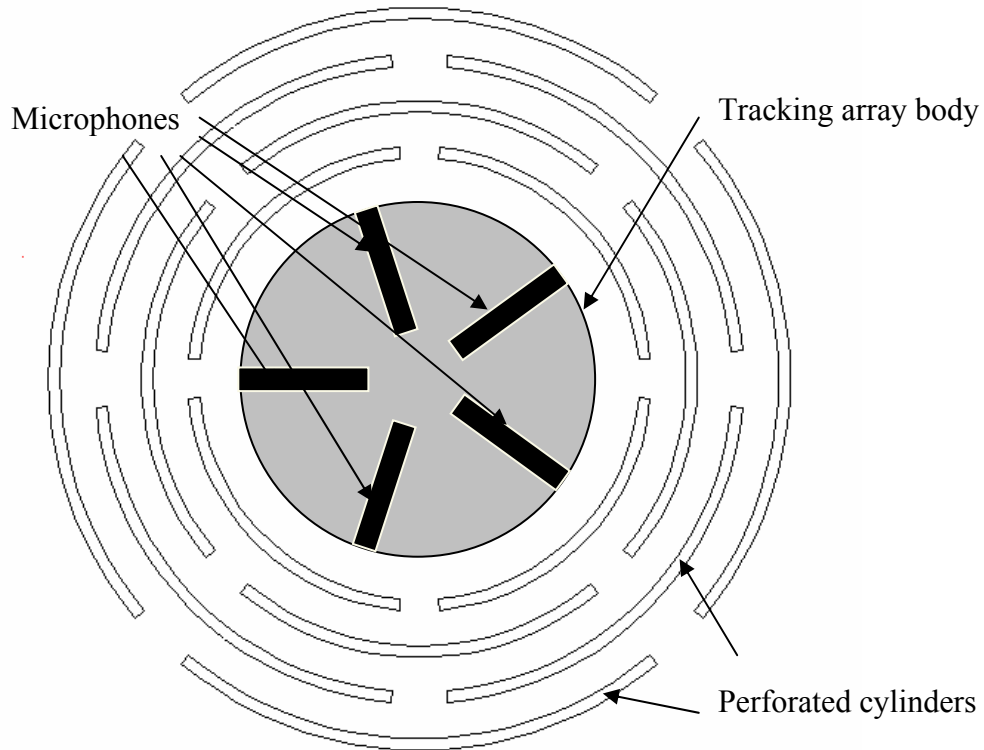


Figure 4-1 Original perforated cylinder concept

The perforations would lower the wind speed enough that any particles in the air would fall out before reaching the microphones. Again, this concept was rejected because it would shift the phase at the microphones. A sound wave traveling through the perforations would have to travel further to some microphones than others. The cone windscreen uses the same idea as the perforated cylinders, but forces the sound wave to travel the same effective distance to all the microphones.

4.2 BASIC GEOMETRY

The cone windscreen design is composed of two concentric cones surrounding the array of five microphones, as shown in Figure 4-2 . The cones are vertically offset in

order to create an air passage for sound waves to reach the microphones. The slant of the cones force particles downward, away from the foam and microphones. In this figure, h is defined as the overlap, w is the gap, and θ is the cone angle. A 3-D view of the windscreen is illustrated in Figure 4-3.

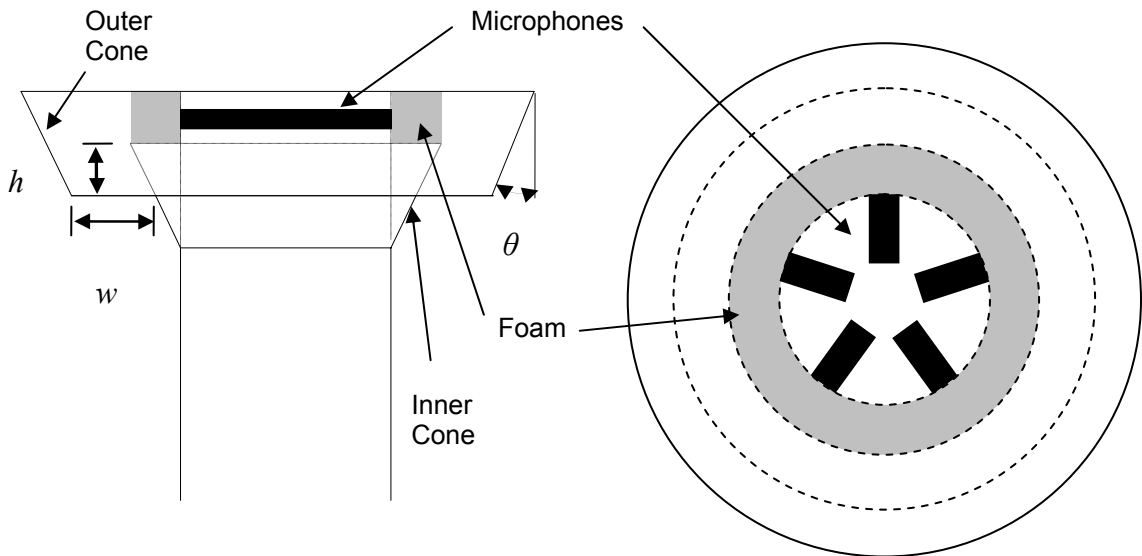


Figure 4-2 2-D side and top view of conical windscreen

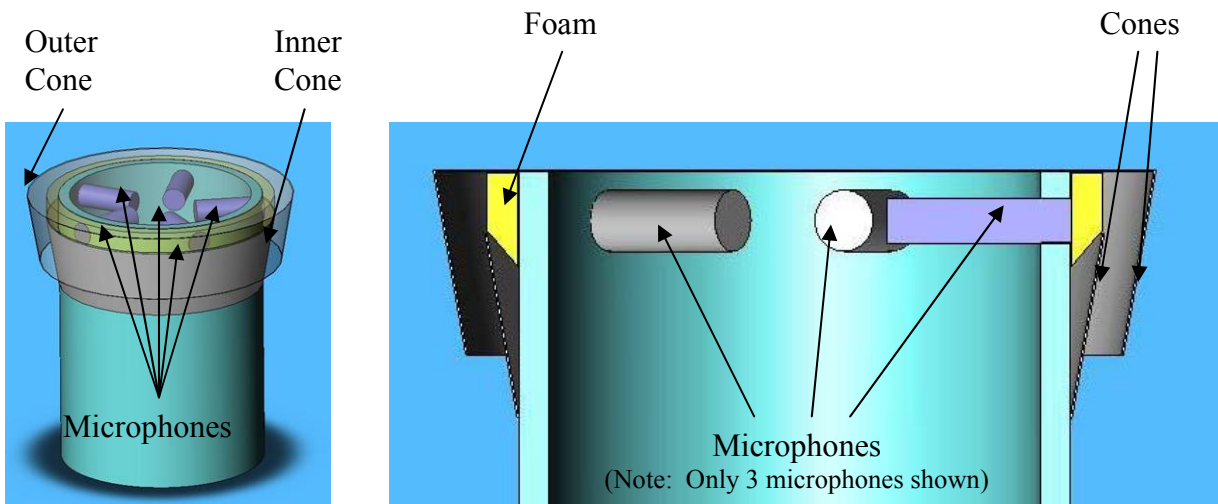


Figure 4-3 CAD drawings of windscreen design

4.3 CFD MODELING RESULTS

Multiple designs were modeled in FLUENT, both 2-D and 3-D. As mentioned previously, it was not time effective to test the insertion loss or the phase shift using CFD modeling; however, they were tested experimentally. From the modeling, it was determined that the angle of the cones should be less than 45° , the overlap of the cones should be between 0.0 and 2.0 inches, and the gap between the cones should be less than 1.5 inches. These values were based on the velocity reduction at the microphones and the amount of sand that entered windscreens.

All windscreens modeled in the CFD package, regardless of geometry, had an acceptable wind velocity reduction. Particles began to enter the windscreen when the overlap was at 0.5 inches, and the gap between the cones was 1.5 inches. This is shown in Figure 4-4, where the outer cone has been removed so the particles entering the windscreen can be seen. With larger overlap and/or smaller gap, no particles entered the windscreen.

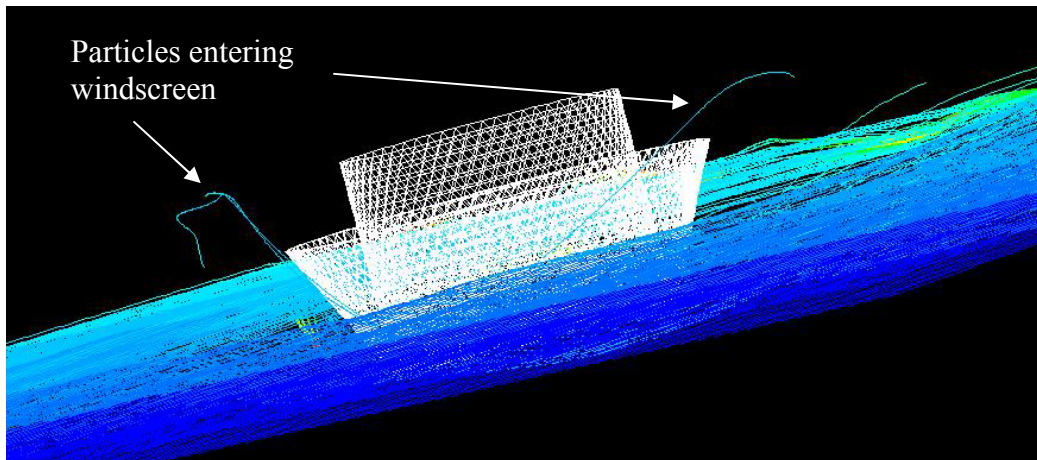


Figure 4-4 Sand insertion for Overlap = 0.5 inches, Gap = 1.5 inches

The values that were determined analytically were used to build prototypes and experimentally test each geometric configuration. Once a final, optimized geometry was determined, a CFD package was again used to model the velocity field and the particle entrapment. In Figure 4-5, a 35 mph wind is simulated flowing over a worst-case scenario of the windscreen and cylinder. Normally, there would be a pressure node at the microphone, so there would be no apparent velocity. To simulate the worst-case scenario, holes were placed so air could travel through the cylinder and out the other side. Obviously, this would not be an accurate model, but even in this case, there was very little wind entering the windscreen.

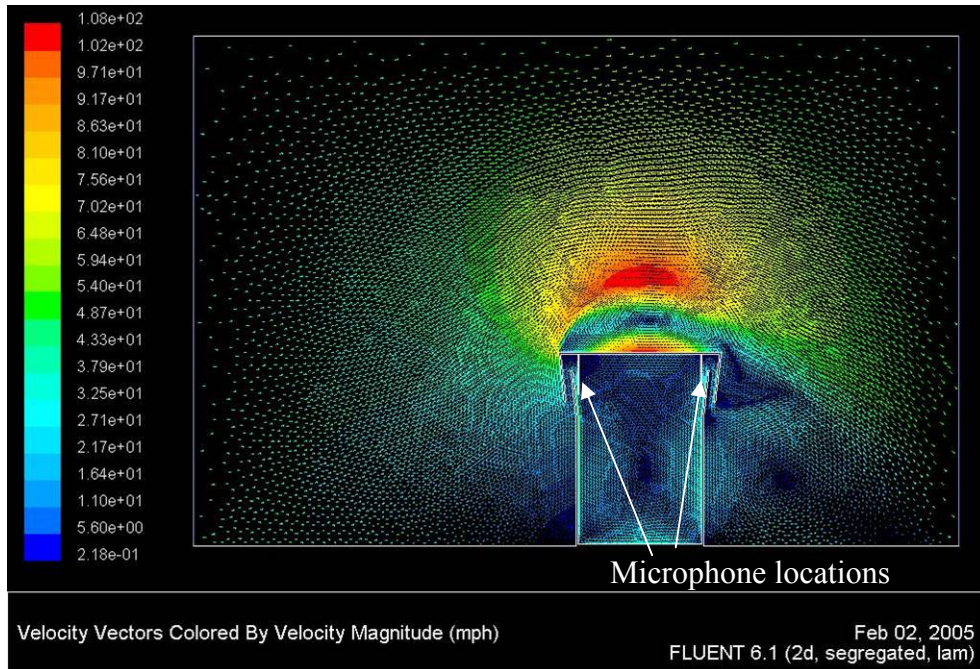


Figure 4-5 2-D CFD modeling of final cone windscreen

Using this same worst-case model, particles were inserted into the velocity stream. Figure 4-6 confirms that, even though there is some air flowing through the

windscreen, none of the particles enter the windscreen. The CFD package was used only to determine the basic design of the windscreen. The geometry was then further optimized through experimental testing.

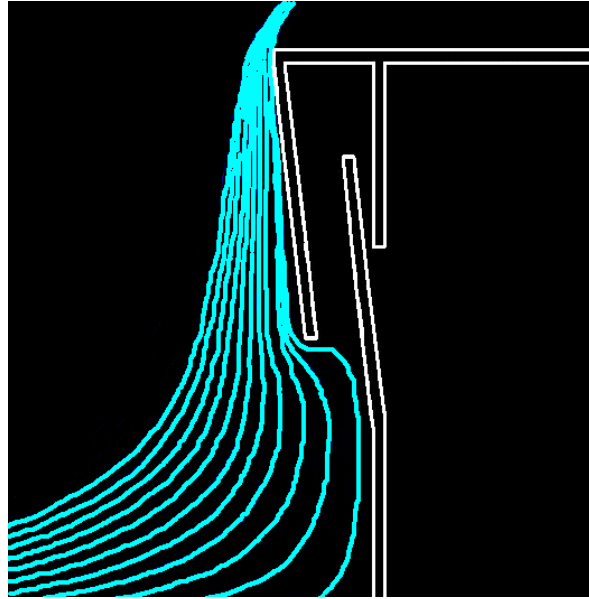


Figure 4-6 2-D CFD modeling of particles with final cone windscreen

4.4 EXPERIMENTAL RESULTS

4.4.1 Factorial Designs

In order to determine the optimal design for a conical windscreen, factorial experiments were performed. The four variables of interest: θ (angle of the cone), w (width of the gap between the cones), h (height of the overlap of the cones), and the amount of foam to be used inside the windscreen as shown in Figure 4-2.

Two different factorial experiments were performed on the conical windscreen. The values of the first are shown in Table 4-1. Using these values, none of the variables

were statistically significant, so a second factorial experiment was performed, which yielded more useful results. The values for the second factorial experiment are shown in

Table 4-2.

Table 4-1 First conical experiment values

	Overlap	Gap	Angle	Foam
Low	1.0 in	1.5 in	45.0°	1.0 in
High	0.0 in	0.5 in	0.0°	0.0 in
Center	0.5 in	1.0 in	22.5°	0.5 in

Table 4-2 Second conical experiment values

	Overlap	Gap	Angle	Foam
Low	2.0 in	0.5 in	20°	1.0 in
High	1.0 in	0.125 in	0°	0.0 in
Center	1.5 in	0.3125 in	10°	0.5 in

Using the high, low, and center values for each variable, four different experiments were performed, and the effect of each variable on the desired output was determined. Following are the tests performed and the results of each.

4.4.2 Wind Noise Attenuation Results

Table 4-3 contains the wind noise attenuation data for two repetitions of the 2⁴ factorial experiment. The last two columns are the results from the two different trials.

A positive value for wind noise attenuation indicates the wind noise without the windscreen is higher than the wind noise with the windscreen. The geometry values are given, along with the wind noise attenuation, which varies from -3 to 9 dB attenuation. One windscreen actually increased the noise by up to 3 dB, while the others attenuated up to 9 dB.

Table 4-3 Wind noise attenuation factorial experiment values

Angle	Overhang	Gap	Foam	Wind Noise Attenuation (dB)	
0°	1.0 in	0.125 in	0.0 in	6	7
20°	1.0 in	0.125 in	0.0 in	6	5
0°	2.0 in	0.125 in	0.0 in	8	9
20°	2.0 in	0.125 in	0.0 in	8	6
0°	1.0 in	0.5 in	0.0 in	-3	-2
20°	1.0 in	0.5 in	0.0 in	0	1
0°	2.0 in	0.5 in	0.0 in	4	3
20°	2.0 in	0.5 in	0.0 in	7	7
0°	1.0 in	0.125 in	0.5 in	9	9
20°	1.0 in	0.125 in	0.5 in	5	5
0°	2.0 in	0.125 in	0.5 in	8	9
20°	2.0 in	0.125 in	0.5 in	9	7
0°	1.0 in	0.5 in	0.5 in	5	6
20°	1.0 in	0.5 in	0.5 in	3	3
0°	2.0 in	0.5 in	0.5 in	8	9
20°	2.0 in	0.5 in	0.5 in	8	8
10°	1.5 in	0.3125 in	0.25 in	2	2
10°	1.5 in	0.3125 in	0.25 in	5	4

After performing statistical analysis on these data, only the angle was deemed insignificant. As intuition would suggest, more foam inside the windscreen increases the wind noise attenuation, as does increasing the overlap of the cones. Decreasing the gap between cones will also increase the wind noise attenuation.

4.4.3 Particle Entrapment Testing Results

Table 4-4 lists the amount of sand trapped while testing each windscreen design. To understand the reduction that has already taken place, the same experiment was performed using a ring of foam around the microphones, rather than a conical windscreen. 38.5 grams of sand were entrapped in the foam after four minutes in the sand blaster. In comparison, the conical windscreen at the center values (10° angle, 1.5 in overhang, 0.32 in gap, and 0.25 in foam) averaged only 0.7 grams of sand trapped during the same time frame. This gives a reduction of over 98%. Each test was repeated, and as shown, there was high variability in each windscreen design. However, it must be remembered that 1 gram of sand is very little, and even 10 grams of sand is little more than a pinch of sand.

Table 4-4 Sand testing factorial experiment values

Angle	Overhang	Gap	Foam	Sand (g) (2 runs)	
0°	1.0 in	0.125 in	0.0 in	6.7	0.7
20°	1.0 in	0.125 in	0.0 in	1.1	1.5
0°	2.0 in	0.125 in	0.0 in	1.6	1
20°	2.0 in	0.125 in	0.0 in	2.5	5.5
0°	1.0 in	0.5 in	0.0 in	53.4	35.7
20°	1.0 in	0.5 in	0.0 in	9.8	4.7
0°	2.0 in	0.5 in	0.0 in	4.6	8.4
20°	2.0 in	0.5 in	0.0 in	8.8	6.3
0°	1.0 in	0.125 in	0.5 in	0.7	1.8
20°	1.0 in	0.125 in	0.5 in	0.9	1.2
0°	2.0 in	0.125 in	0.5 in	0.8	1.2
20°	2.0 in	0.125 in	0.5 in	1	5.5
0°	1.0 in	0.5 in	0.5 in	0.5	0.7
20°	1.0 in	0.5 in	0.5 in	1.2	3
0°	2.0 in	0.5 in	0.5 in	4.1	0.8
20°	2.0 in	0.5 in	0.5 in	5.2	6.4
10°	1.5 in	0.3125 in	0.25 in	0.5	0.9

4.4.4 Insertion Loss Testing Results

The insertion loss of the windscreen was also tested using a 2^4 factorial design. The testing was done at 11 different frequencies ranging from 50-10,000 Hz. The data show that there is negligible insertion loss for every cone value up to 2,000 Hz. Therefore, none of the variables were significant, in the range tested, so the size and shape of the conical windscreen does not effect the insertion loss. Figure 4-7 graphs the insertion loss of an average cone windscreen as a function of input frequency, compared to different thicknesses of commercial foam.

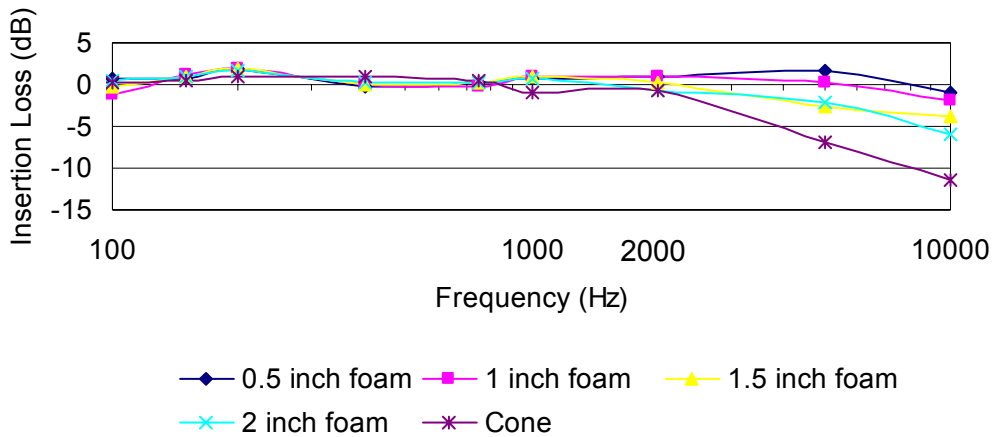


Figure 4-7 Insertion loss of cone different foam windscreens

The cone windscreen is identical to the foam windscreens until 1000 Hz, at which point it rolls off faster than does the regular foam. The average difference between 1.5 inches of foam and the cone windscreen from 100-1000 Hz is 0.15 dB, which is statistically insignificant. Because this technology will only be applied at frequencies under 1000 Hz, the roll-off is not considered an issue for concern.

4.4.5 Phase Shift Testing Results

For the factorial experiments, only two of the five possible microphones were used to test for phase shifting. These were set 90° apart from each other. Unfortunately, during the preliminary factorial experiments, the cone windscreen acted like a Helmholtz resonator (the pressure throughout the windscreen was the same, regardless of location), which drastically changed the phase between the microphones. To overcome this problem, dividers were added between each microphone, as shown in Figure 4-8. Adding these dividers to the cone decreased the phase shift error a substantial amount.

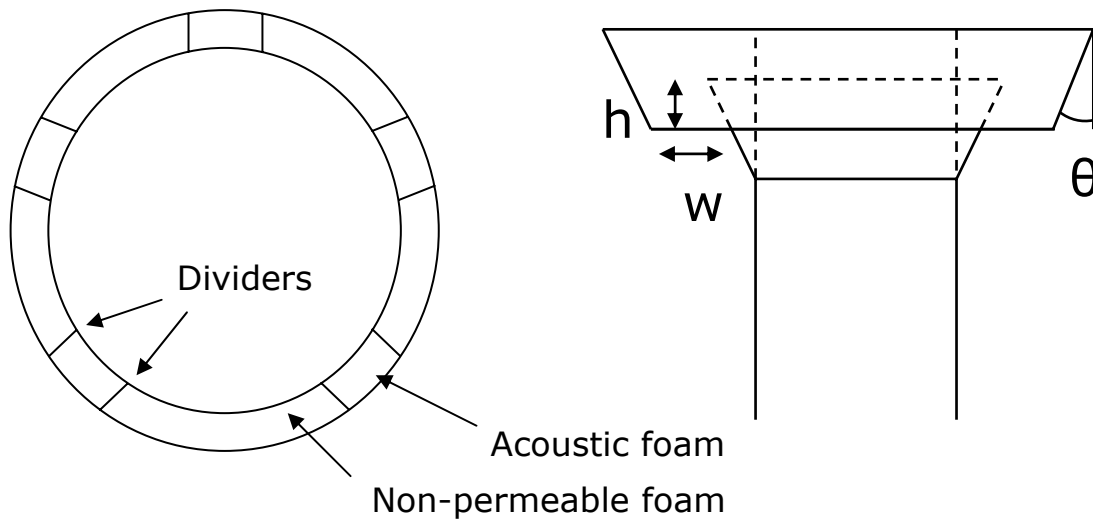


Figure 4-8 Dividers for phase change control

The dividers were made by inserting metal dividers, and then filling the gaps outside of the desired path with non-permeable foam. Non-permeable foam was chosen to decrease the amount of sound transferred through the windscreen. Table 4-5 shows the

error before and after the dividers. Adding the dividers decreases the average error from over 100%, to 3.28%.

Table 4-5 Phase difference error for cones with/without dividers

	Average % error (50-1000 Hz)	Average error (Degrees)	Max % error (50-1000 Hz)	Max error (Degrees)
Without Dividers	103.40%	41.88°	275% (at 1000 Hz)	152° (at 1000 Hz)
With Dividers	3.28%	1.56°	12% (at 200 Hz)	4.15° (at 900 Hz)

4.5 FINAL DESIGN

4.5.1 Final Geometry

To determine the optimal design, the data from each of the four tests were used. Foam always caused better results, so it is set at its highest value. The other values were chosen for structural support, size, and acoustical properties. Table 4-6 shows the optimal geometric values for the conical windscreen.

Table 4-6 Optimal conical configuration values

	Optimal
Angle	10°
Overhang	1 in
Gap	0.3125 in
Foam	0.5 in

All of the factorial testing was done using two Larson-Davis pre-polarized condenser microphones. After choosing the optimal design, further testing was done using new 1" diameter microphones built specifically for this application. Because of their size, all five microphones were able to fit inside the cylinder, and a new windscreen was built that incorporated all five microphones. This windscreen is shown in Figure 4-9. As shown, the windscreen has been covered with a Gortex cloth. Testing was done with two configurations: covering the outside of the cone with Gortex, as shown, and covering everything with Gortex, including the foam-filled slots.

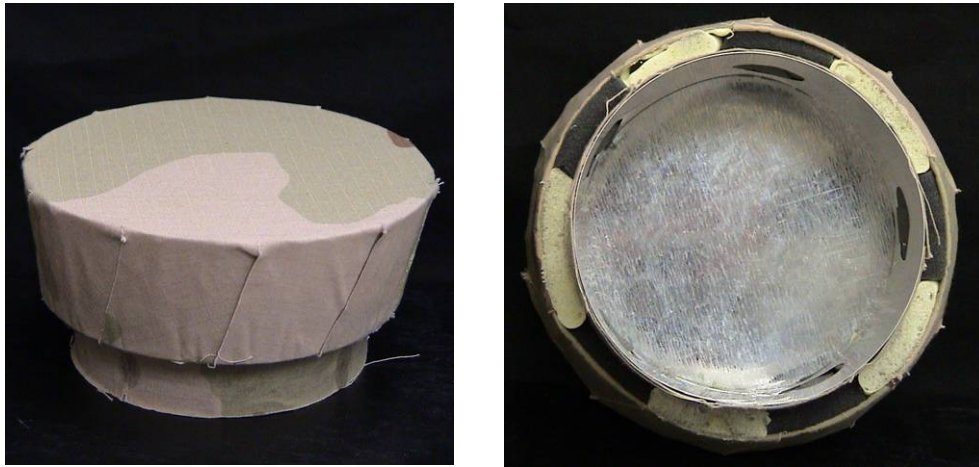


Figure 4-9 Final conical windscreen prototype

Using this new windscreen, the four tests were performed again. Because this was the final prototype, more detailed tests were performed. For example, the phase was measured over the entire 360° surface of the windscreen, rather than just at one location. Other tests were changed slightly because of the extra weight of the microphones.

4.5.2 Final Results

A prototype was built using the geometric values given in Table 4-6. Each test was performed again to insure that all design criteria were satisfied. Table 4-7 shows the results of these tests, compared to a commercial windscreen of 1.5 inches of foam. This final prototype performed better than the previous prototype in two tests, wind noise attenuation and phase shift. The wind noise attenuation improved from 8.0 dB to 9.1 dB at 13 mph. The phase shift was lowered from 3.28% to under 3.00%. These reductions were probably caused by the increased precision in the geometry of the prototype.

Table 4-7 Optimal conical final values

	Cone	1.5" foam
Wind noise attenuation	9.1 dB	8.1 dB
Insertion Loss	< 0.4 dB	< 0.4 dB
Sand	0.1 g	38.5 g
Phase	< 3% error	≈ 0% error

Figure 4-10 shows the wind noise attenuation of the final cone windscreen, compared to the microphone array without a windscreen at 13 mph. As shown, although there are some dominant frequency peaks caused by the fan, there is still an obvious wind noise attenuation of about 9.1 dB, which is higher than the previous wind noise attenuation measured.

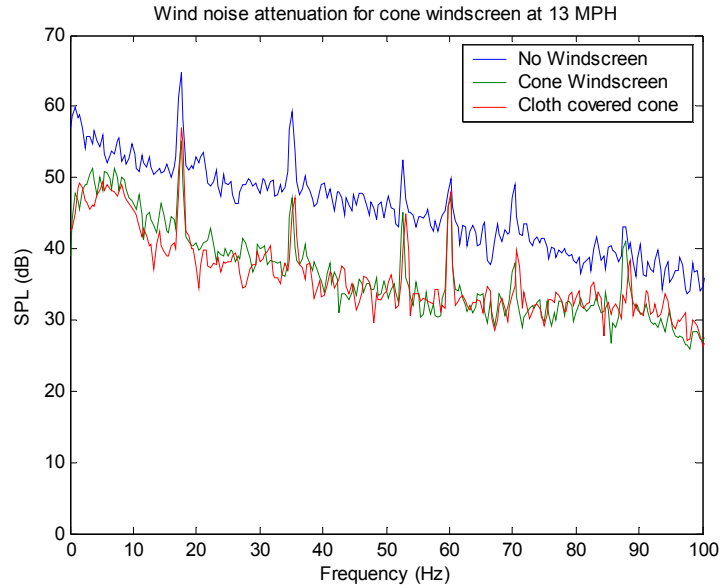


Figure 4-10 Wind noise attenuation for the final conical windscreen at 13 mph

Figure 4-11 is zoomed in from 20 to 70 Hz, over which frequency there is a 9.9 dB wind noise attenuation. Using a faster, yet louder fan, wind speeds up to 20 mph were obtained. At 20 mph, the wind noise attenuation was 16.7 dB, as shown in Figure 4-12. The trend of higher attenuation vs. higher wind speed is expected to continue for even higher speeds.

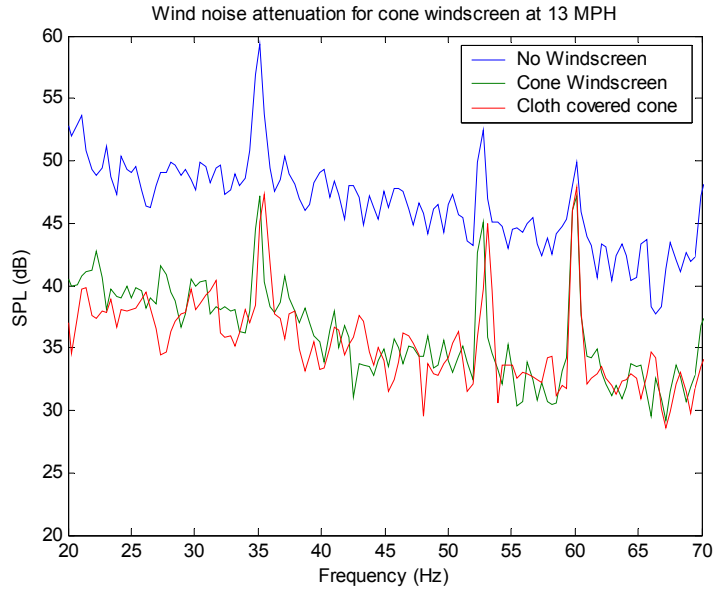


Figure 4-11 Wind noise attenuation for the final conical windscreen at 13 mph (zoomed in)

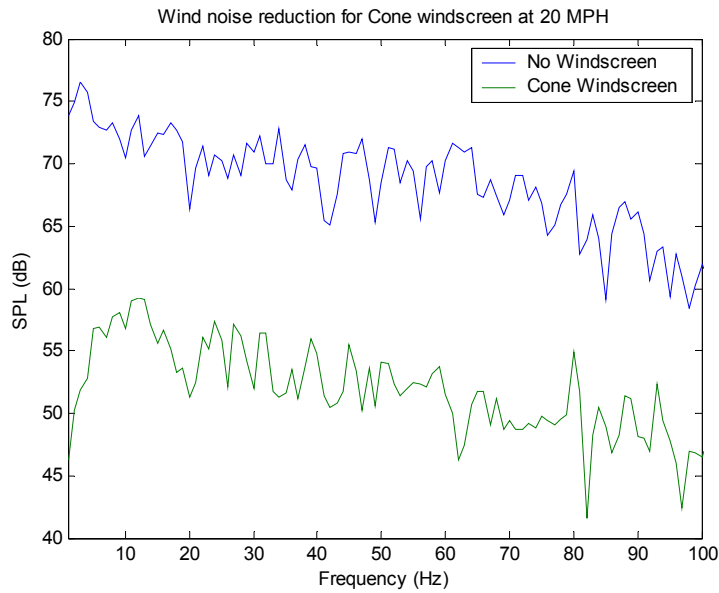


Figure 4-12 Wind noise attenuation for the final conical windscreen at 20 mph

Using the five microphone setup, a 360° phase error plot was constructed. Although the measurements were taken in a similar fashion, the windscreen was rotated through 72°, rather than only using two microphone readings, located 90° apart. Using all five microphones, the full 360° error plot was extrapolated. In Figure 4-13, the error between the microphone array with and without the cone windscreen is shown. The sound source was located at 0°, and as illustrated, all errors are less than 3%.

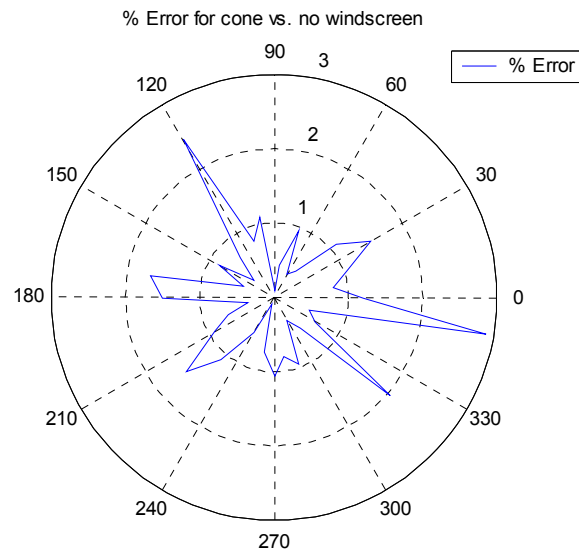


Figure 4-13 360° phase error plot for cone windscreen

The final geometric specifications are shown in Figure 4-14. Using this geometry and the five microphone array with the cone windscreen, the results in Table 4-8 were determined. These results compare the cone windscreen to 1.5 inch foam.

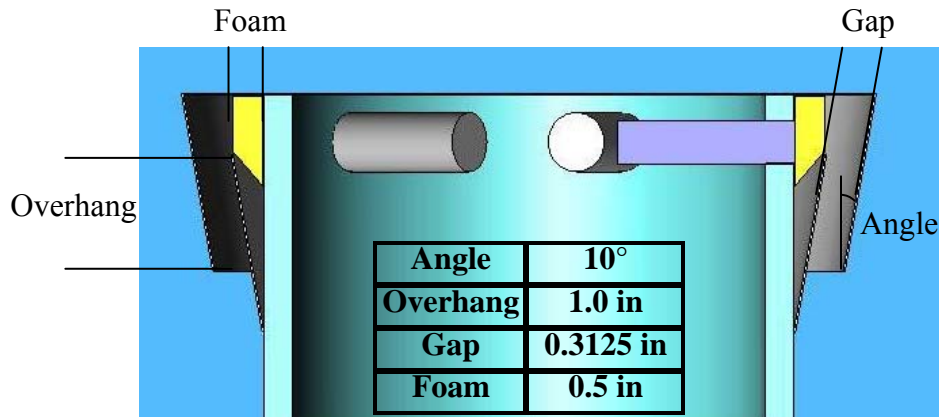


Figure 4-14 Final cone windscreen geometry

Table 4-8 Optimal conical final values

	Cone	1.5" foam
Wind noise attenuation (13 mph)	9.1 dB	8.1 dB
Wind noise attenuation (20 mph)	16.7 dB	15.0 dB
Insertion Loss	< 0.4 dB	< 0.4 dB
Sand	0.1 g	38.5 g
Phase	< 3% error	≈ 0% error

5 SPIDER WINDSCREEN

5.1 OVERVIEW

In this chapter, the spider windscreen design is explained. First, the reasoning behind the spider windscreen is given along with the explanation of its geometry. Analytical and experimental results are the focus of this chapter. Topics are addressed in this chapter as follows:

- Basic geometry
- CFD modeling results
- Experimental results
- Final design

5.2 BASIC GEOMETRY

The spider windscreen design was formulated when dividers were needed to control the phase shift in the conical windscreen design. The dividers effectively created slots for the sound to reach each microphone individually. The spider windscreen removes the cone and utilizes only the individual paths for each microphone, as shown in Figure 5-1.

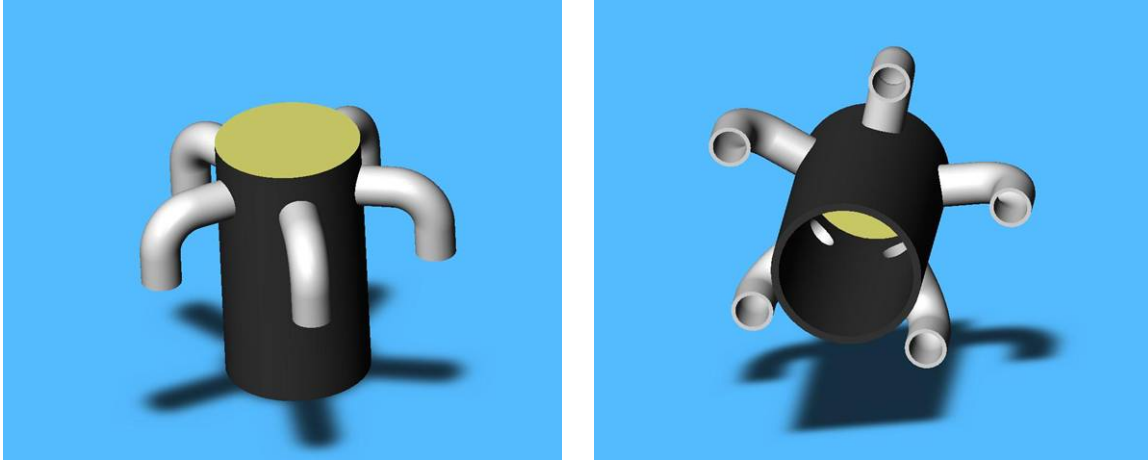


Figure 5-1 Spider windscreen design

Tubes are rigidly attached to the cylinder directly around the microphone. Each tube is then filled with foam to increase the wind noise attenuation. Three parameters were tested using a CFD package; g , the tube gap at the entrance of the tube, L , the length of the tubes, and D , the tube diameter. The only variable that was not altered was w , the distance the tube protrudes from the cylinder. These four variables are shown in Figure 5-2.

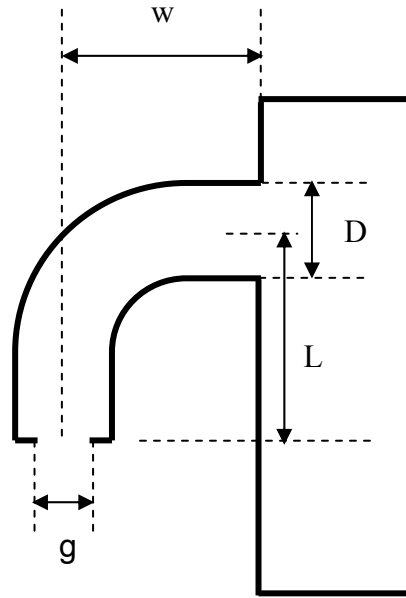


Figure 5-2 2-D view of spider windscreen variables

5.3 CFD MODELING RESULTS

A CFD package was used to determine the basic geometry of the spider windscreen. 2-D models were created to determine the tube gap, the length of the tube, and the tube diameter that would decrease wind velocity at the microphone diaphragm and reduce the amount of particles entering the tube. Tube lengths varied from 0.5 inches to 2.0 inches, the tube gap was varied from the tube diameter to 0.25 inches smaller than the tube diameter, and the tube diameter was varied from 0.5 inches to 1.0 inch. The tube protrusion was held constant at 1.5 inches to simplify the experimentation.

Figure 5-3 show two different tubes in 35 mph flow fields. Figure 5-3a is the most conservative model in that the flow is blocked from passing through the tube by sealing off any passage out of the tube. Figure 5-3b shows a non-conservative scenario, in that the bottom of the cylinder is left open, which allows the most amount of air to

flow through the tube. Even with this scenario, the velocity at the microphone is negligible. In the actual application, the tube would be mostly or completely sealed, similar to Figure 5-3a, and therefore much less wind would be able to pass through the tubes.

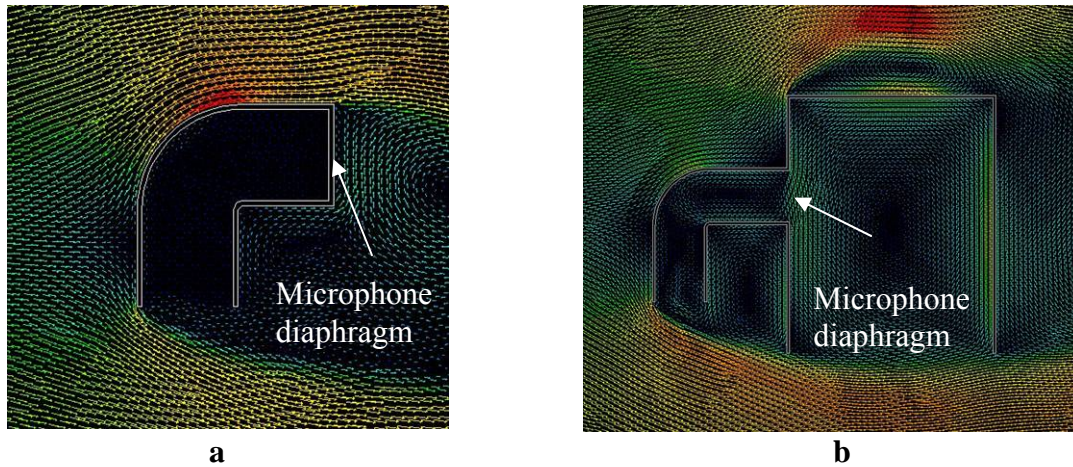


Figure 5-3 CFD simulations of velocity reduction in a spider windscreen

In the CFD models, the tube gap, the tube diameter, and the length of tube did not affect the reduction of the wind significantly. Each model was very good at reducing the wind speed, including those that allowed much more flow than would actually happen.

Figure 5-4 contains a view of the lower end of one tube where particles have been inserted into a 35 mph flow. Even when there is some velocity flow up the tube, none of the particles enter the base of the tube. From this, we can expect the spider windscreen to be exceptional at reducing the amount of particles entering the windscreen.

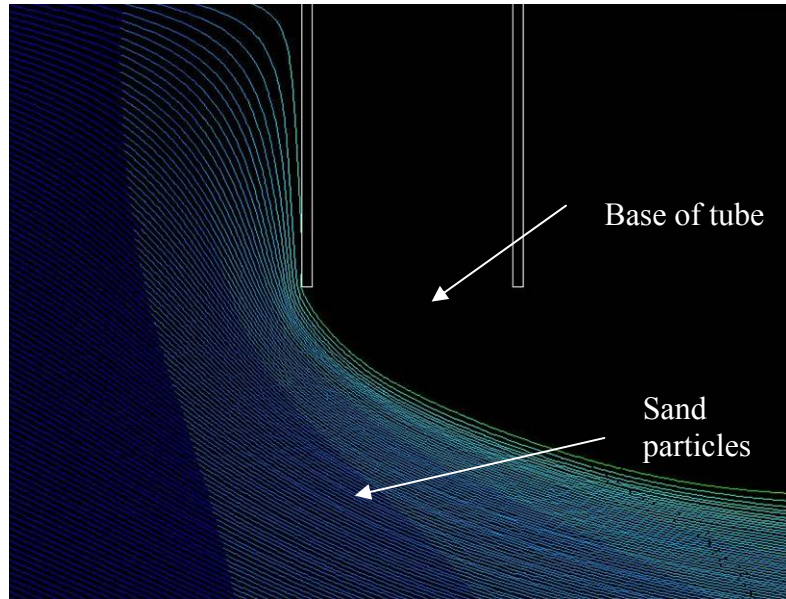


Figure 5-4 CFD simulation of particles hitting a spider windscreen

5.4 EXPERIMENTAL RESULTS

Testing was done on the spider windscreen under a number of conditions. The length of the tube was changed, along with covering the tube ends with a Gortex material, provided by Kevin Malone at Sandia National Laboratories. The following sections explain the tests performed for wind noise attenuation, particle entrapment, insertion loss, and phase shift error, with the focus on the results of each of these experiments.

5.4.1 Wind Noise Attenuation Results

The spider windscreen was tested for wind noise attenuation in a similar manner to the cone windscreen. The spider was placed in front of an axial fan blowing at 13 mph. The attenuation in wind noise was measured and compared to the measurements collected by the microphone array without a windscreen. As shown in Figure 5-5, the spider windscreen does not lower the wind noise by a significant amount, averaging only

1.3 dB of wind noise attenuation. However, when the end is covered with a Gortex cloth, the average wind noise attenuation reaches 8.9 dB. This approaches the attenuation obtained by current foam windscreens. One possible explanation for the low wind noise attenuation is that greater turbulence is caused by the flow around the tube ends. By covering the tube ends with a cloth, the amount of that turbulence that reaches the microphone is reduced.

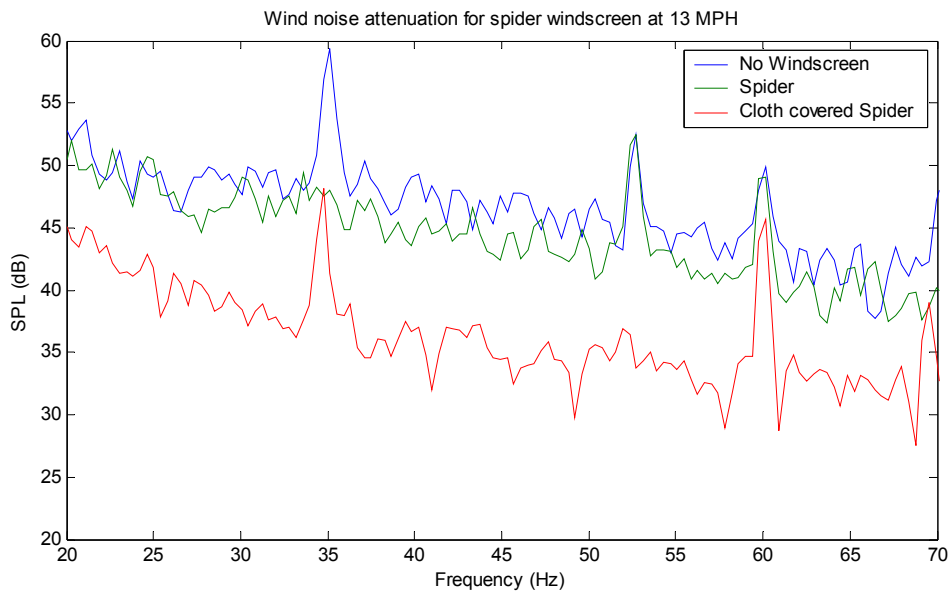


Figure 5-5 Wind noise attenuation for a spider windscreen

Using a faster, yet louder fan, wind speeds up to 20 mph were obtained. The dominant peaks in this fan differ from the 13 mph fan and it has a much higher broadband noise. At 20 mph, the wind noise attenuation was 16.7 dB, as shown in Figure 5-6. This trend of higher attenuation vs. higher wind speed should continue for even higher wind speeds.

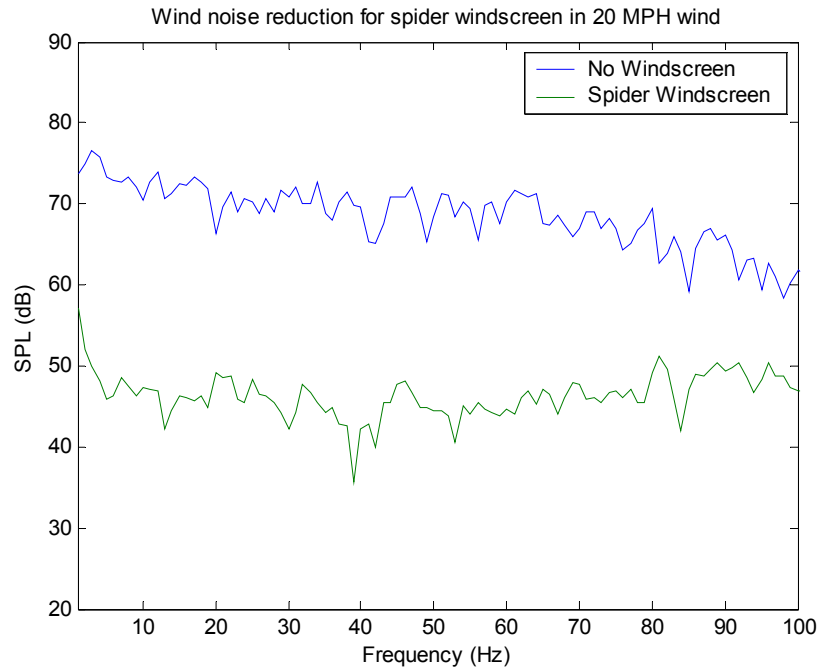


Figure 5-6 Wind noise attenuation for a spider windscreen with cloth at 20 mph

5.4.2 Particle Entrapment Testing Results

Particle entrapment testing confirmed the results computed when using the CFD modeling. The same sand blaster was used to test the spider windscreen as the conical windscreen. The results of each test, regardless of the tube length, diameter, covering, or amount of foam, were the same. There was never more than 0.1 g of sand in the windscreen, which is the smallest amount possible to measure.

In Figure 5-7, the spider windscreen is shown positioned in the sand blaster. Even when the windscreen was tested for more than the nominal four minutes, no more than 0.1 g of sand entered the tubes.



Figure 5-7 Particle testing for a spider windscreen

5.4.3 Insertion Loss Testing Results

Similar to the cone windscreen, the spider windscreen has negligible insertion loss. All measured values fall within the noise of the system. Figure 5-8 is the insertion loss for the Spider windscreen, from 100 to 10,000 Hz. Similar to the cone windscreen, above 1000 Hz the insertion loss starts to become large.

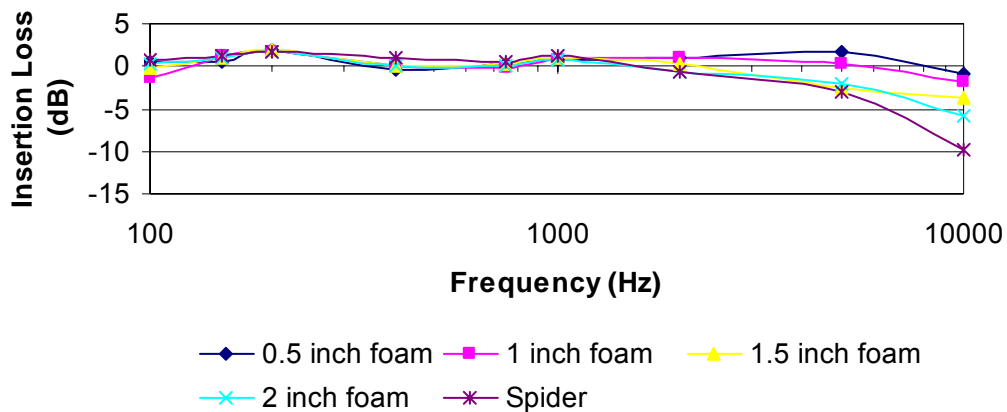


Figure 5-8 Insertion loss for a spider windscreen

5.4.4 Phase Shift Testing Results

The phase change between the microphones is one of the great benefits of using the spider windscreen. Because the tube ends are further out than the actual microphone diaphragms, the effective diameter is enlarged. This will increase the ability of the array to be used to locate the direction of a sound. In Figure 5-9, the error between the final spider windscreen and the array without a windscreen is shown. The sound source was located at 0° , and as shown, the error is never more than 2%.

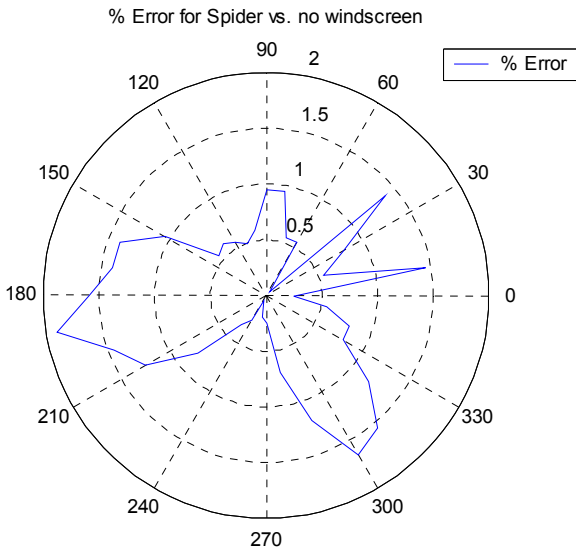


Figure 5-9 360° phase error plot for a spider windscreen

5.5 FINAL DESIGN

5.5.1 Final Geometry

Preliminary testing made it appear that the size and shape of the spider windscreen was not important, as long as the tube ends are covered. A final prototype made with 1 inch diameter tubes and a tube length of 1 inch was constructed. The tube ends were covered with Gortex, and each of the four tests were performed again. This final geometry is shown in Figure 5-10.

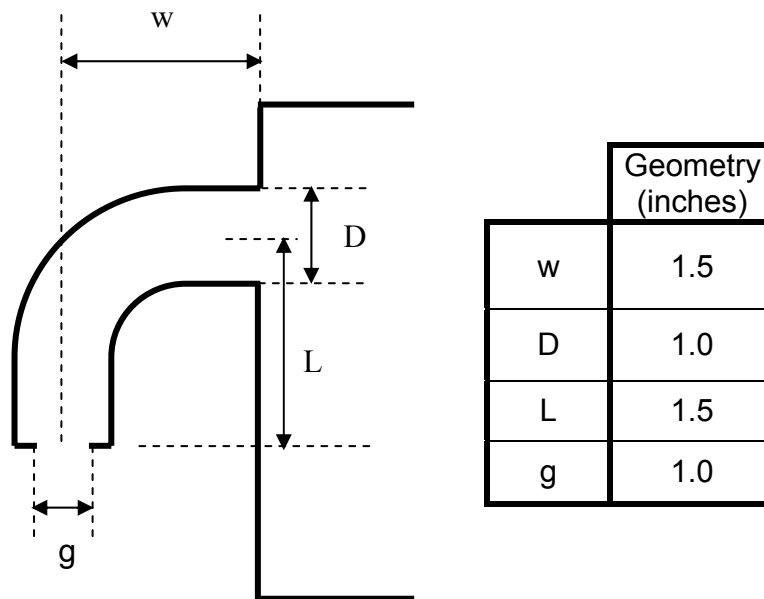


Figure 5-10 Final spider windscreen geometry

5.5.2 Final Results

The results from the four tests were the same as those determined previously, as shown in Table 5-1. From this table, it is shown that the spider windscreen design

exceeds all of the design criteria. At high wind speeds, the spider becomes much better than even commercial foam at wind noise attenuation.

Table 5-1 Optimal spider final values

	Spider	1.5" foam
Wind noise attenuation (13 mph)	8.9 dB	8.1 dB
Wind noise attenuation (20 mph)	22.2 dB	15.0 dB
Insertion Loss	< 0.4 dB	< 0.4 dB
Sand	< 0.1 g	38.5 g
Phase	< 2% error	≈ 0% error

Because the spider is a secondary design, it has not been tested to the same extent as the cone design. Additionally, factorial testing was not done on the spider windscreen to optimize tube length and tube size. From CFD modeling, it appeared that tube size and length were not significant; however, experimental testing should be performed to verify their insignificance. It may be that the tubes could be significantly smaller in diameter and length.

6 CONCLUSIONS

The goal of this research was to design a windscreen that 1) has a wind noise attenuation of at least 8 dB, 2) protects an array of five microphones from sand and dirt particles, 3) has an insertion loss of no more than 1 dB from 5-1000 Hz, and 4) does not alter the phase difference between each microphone by more than 3% over the same range. Both windscreen designs meet these requirements. Table 6-1 shows these requirements and the result for each windscreen.

Table 6-1 Final results for cone and spider windscreen

	Requirement	Cone	Spider
Wind noise attenuation (13 mph)	> 8 dB	9.1 dB	8.9 dB
Sand reduction	> 90%	> 99%	> 99.8%
Insertion loss	< 1 dB	< 0.4 dB	< 0.4 dB
Phase shift	< 3%	< 3%	< 2%

Another benefit of this research was the exploration of a method for designing microphone windscreens. Both computer modeling and experimental testing were used. A windscreen can easily be modeled in a CAD package, imported into a CFD package, and have the wind speed reduction measured. A CFD package can also quickly model particle flow. The negative aspect of using a CFD package is the difficulty in modeling the insertion loss and phase shift of the windscreen. It is recommended that CFD

modeling only be used for these two criteria if building windscreen prototypes is prohibitively expensive. When experimental prototypes are feasible, it is recommended that they be used to fine-tune the geometry, after using a CFD package to design a basic geometry for the windscreen.

6.1 FINAL DESIGNS

6.1.1 Cone Windscreen

The final geometric values for the cone windscreen are shown in Figure 6-1.

With this geometry, the cone windscreen has the following properties.

- Wind noise attenuation of 9.1 dB at 13 mph, 16.7 db at 20 mph
- Particle reduction of 99%, from 38.5 g (in foam) to 0.1 g
- Average insertion loss of less than 0.4 dB
- Maximum phase shift error of less than 3%

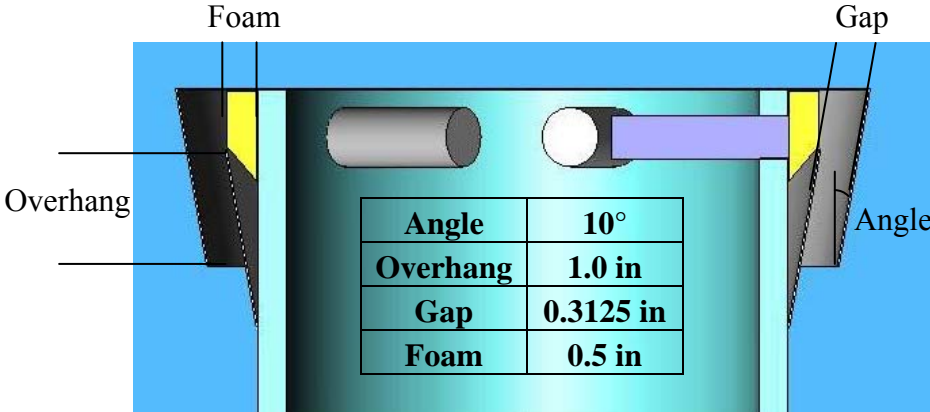


Figure 6-1 Final cone windscreen geometry

6.1.2 Spider Windscreen

The final geometric values for the spider windscreen are given in Figure 6-2.

With this geometry, the spider windscreen has the following properties.

- Wind noise attenuation of 8.9 dB at 13 mph, 22.2 dB at 20 mph
- Particle reduction of 99%, from 38.5 g (in foam) to less than 0.1 g
- Average insertion loss of less than 0.4 dB
- Maximum phase shift error of less than 2%

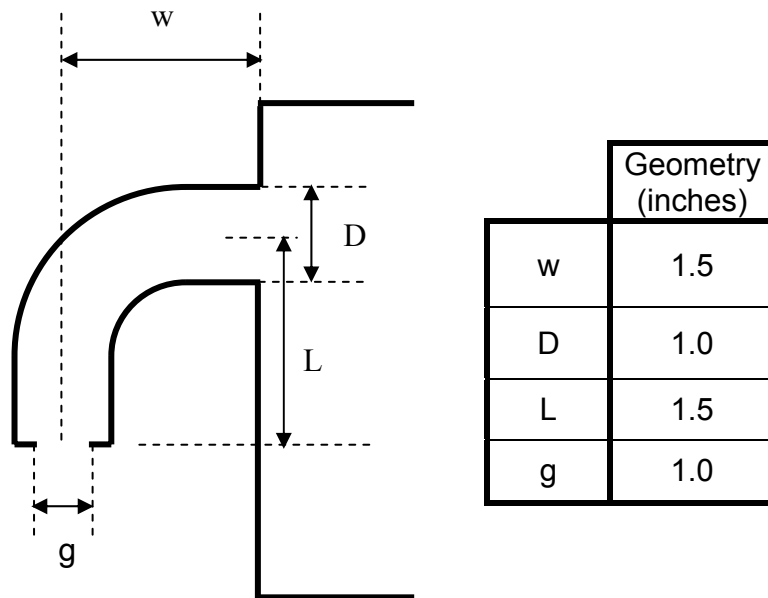


Figure 6-2 Final spider windscreen geometry

6.2 RECOMMENDATIONS FOR FURTHER RESEARCH

Both windscreens meet the desired requirements, though more testing has been done on the cone windscreen than the spider. Two main areas of research still need to be explored. First, more detailed experimentation can be done on the spider windscreen. A 2⁴ factorial test should be done to determine if the tube lengths and gap are significant,

along with the protrusion length and the inside tube diameter. By changing the protrusion length of the tubes, the phase difference between the microphones can be changed. The second future research topic is to determine how changing the phase affects the ability of the locating algorithm in finding the noise source. Some questions that could be answered are:

- How many microphones should be used to find the noise source?
- How spread out should the microphones be for the best convergence?
- What should the geometry of the microphone array be to best find the source?

6.3 PUBLICATIONS

A paper was presented at the 148th Meeting of the Acoustical Society of America, November 15-19, 2004. It is also expected that a paper will be submitted to the Noise Control Engineering Journal.

REFERENCES

- ¹ Kinsler, L., A. Frey, A. Coppens, and J. Sanders, *Fundamentals of Acoustics, Fourth Edition*. New York: John Wiley & Sons, Inc., 2000.
- ² Bleazey, J.C., “Experimental determination of effectiveness of microphone wind screens,” *Journal of the Audio Engineering Society Organization*, 1961, vol. 9, Issue 1, pp. 48-54.
- ³ Keleman, A., “Windnoise protection of microphones,” *7th International Congress on Acoustics*, 1971, pp. 281-284.
- ⁴ Menge, C.W. and G. Sanchez, “Low-noise windscreen design and performance,” *Noise-Con 94*, May 1-4, 1994. pp. 787-792.
- ⁵ Hosier, R.N., and P.R. Donovan, “Microphone windscreen performance,” *National Bureau of Standard Report 79-1599*, 1979.
- ⁶ Skøde, F., “Windscreening of outdoor microphones,” *Bruel & Kjaer Tech. Rev*, 1966, no. 1, pp. 3-10.
- ⁷ Morgan, S., and R. Raspet, “Investigation of the mechanisms of low-frequency wind noise generation outdoors,” *Journal of the Acoustical Society of America*, 2002, no. 92, pp. 1180-1183.
- ⁸ Wuttke, J., “Microphones and wind,” *Journal of the Audio Engineering Society*, 1992, vol. 40, Issue 10, pp. 809-817.
- ⁹ Schomer, P., R. Raspet, M. Wagner, D. Walker, D. Marshall, and J. Brunner, “Methods for detecting low-frequency signals in the presence of strong winds,” *Construction Engineering Research Laboratory*, Champaign, Illinois, June 29, 1988.
- ¹⁰ Woolf, C., “How to reduce wind noise and vibration,” *Microphone Data Book*, Rycote Microphone Windshields Ltd, 2003.
- ¹¹ Kaye, D., “Sound attenuation by commonly available membranes used for moisture protection of microphones,” *Journal of the Acoustical Society of America*, 1975, no. 6, pp. 1328-1329.

¹² Lawson, J., and J. Erjavec, *Modern Statistics for Engineering and Quality Improvement*. California: Wadsworth Group, 2001.

¹³ Ai, Y., X. Qiu, and C. Hansen, "Minimizing wind effects on active control systems for attenuating outdoor transformer noise," *Noise Control Engineering Journal*, 2000, vol. 48, Issue 4, pp. 130-135.

APPENDIX

APPENDIX

FLUENT TUTORIAL

This tutorial assumes a basic understanding of FLUENT. A list of the steps to perform both the wind noise reduction and particle entrapment tests are given, along with screenshots for most steps.

Wind noise reduction

Once the model has been opened in FLUENT, the wind noise reduction can be modeled. Before a flow is placed around the windscreen, it is necessary to assure that the grid and the output are in the correct units. The steps are outlined below;

- A. Check the units of the grid , as seen in Figure A-1, using: Grid → Scale Grid.

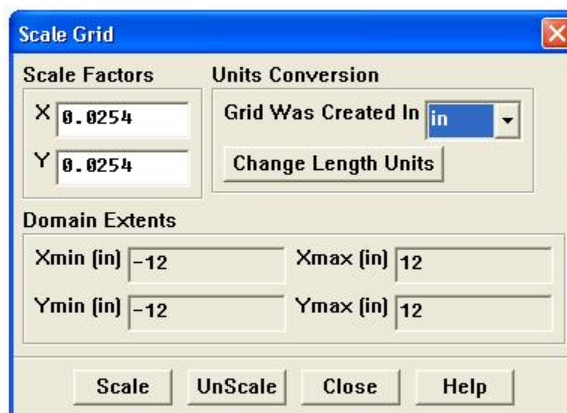


Figure A-1 Scale Grid screenshot

B. Define units for inputs and outputs using: Define → Units

Any of the inputs and/or outputs can be defined in English or SI units, as shown in Figure A-2. In the simulations modeled, the velocity was desired in mph. Other variables, such as length, can be changed to English units if desired, but are not necessary for accurate modeling. SI units are default in FLUENT.



Figure A-2 Set Units screenshot

C. Set velocity inputs and outputs using: Define → Boundary Conditions → Vin

In this scenario, Vin is the velocity in, while Vout is the outward velocity, described as a negative velocity input.

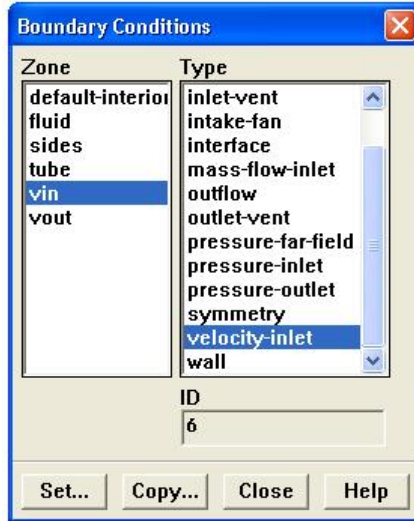


Figure A-3 Boundary Conditions screenshot

Once velocity-inlet is selected, as shown in Figure A-3, push Set..., and the velocity-inlet can be changed, as shown in Figure A-4. The velocity can then be changed. A positive value signifies a flow into the volume, while a negative value signifies a flow out of the volume of interest.

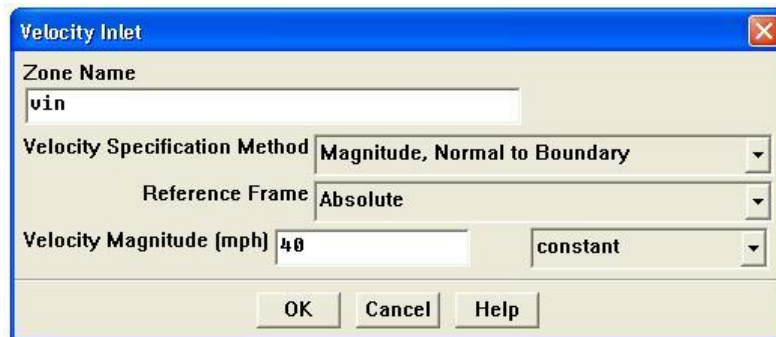


Figure A-4 Velocity Inlet screenshot

D. The velocity field must then be initialized, seen in Figure A-5, using: Solve
→ Initialize → Initialize → Compute From → vin

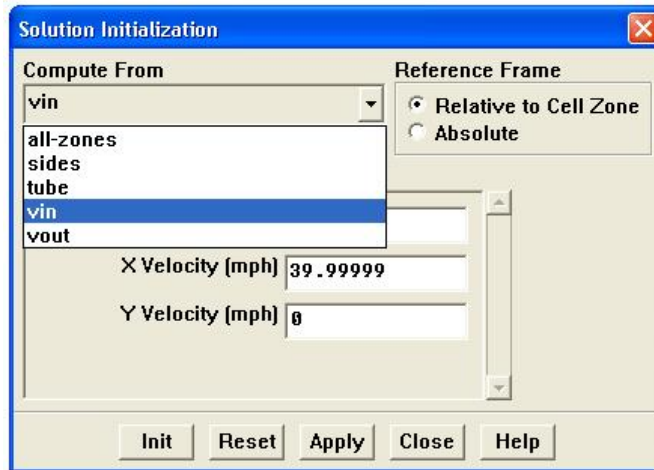


Figure A-5 Solution Initialization screenshot

When the flow is initialized, all nodes are set to the initialization value. In this case, the velocity of the flow at vin was used to initialize the entire flow. The flow can be visualized by using: Display → Vectors → Display

There are many options for visualization, as shown in Figure A-6, though for a velocity flow, the most useful is the plot of velocity vectors, colored by velocity magnitude.

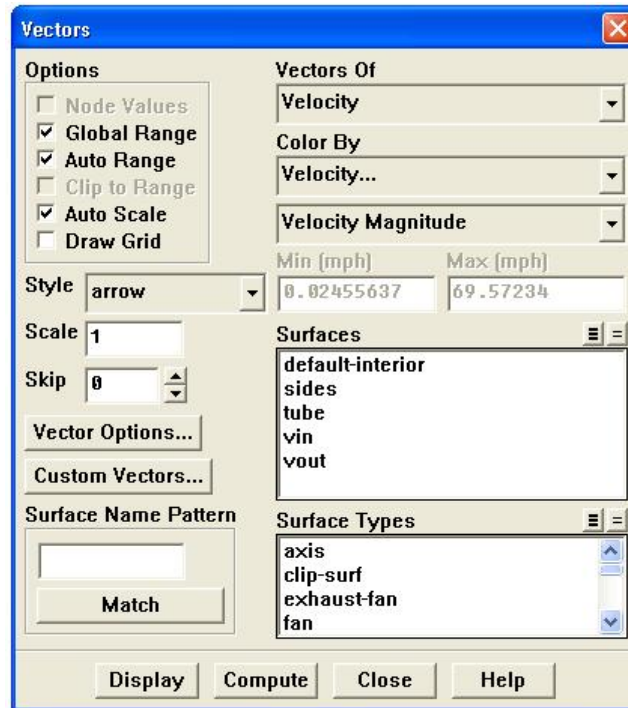


Figure A-6 Vectors screenshot

E. The velocity flow can now be solved using: Solve → Iterate → Iterate

The number of iterations can be increased until the solution is sufficiently converged.

This is shown in Figure A-7. The reporting interval shows how often the results are printed to the screen.

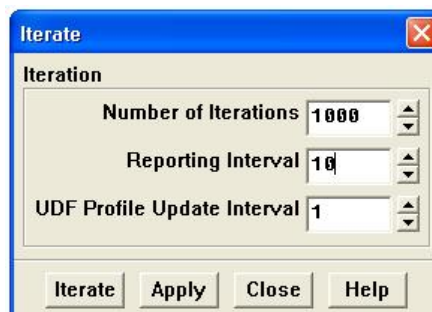


Figure A-7 Iterate screenshot

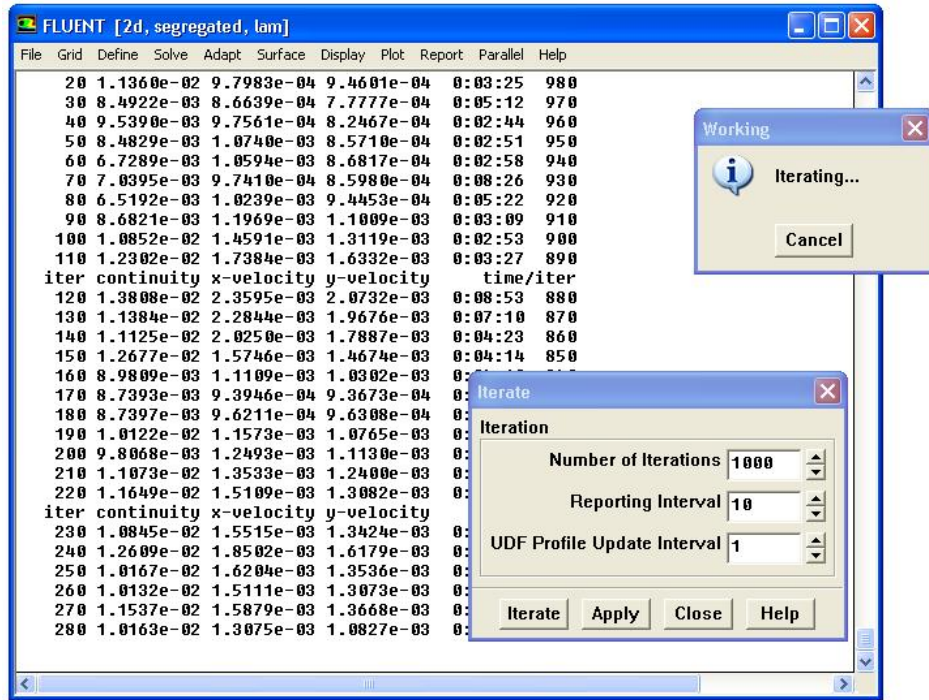


Figure A-8 Iterating screenshot

The report printed to the screen lists the continuity of the model, as shown in Figure A-8. The default convergence criterion is a continuity of less than $1e-04$. This criterion can be used for convergence, or it can be changed by the user. Once the flow is converged, the velocity field can be seen using the vector display already open. To zoom in on the point of interest, click and drag the middle mouse button. The velocity reduction is then calculated by observing the velocity vectors at steady state, and comparing them to the velocity vectors at the microphone.

Particle insertion

F. Once the velocity flow has converged, particles can be inserted into the flow, using: Define → Injections → Create



Figure A-9 Injections screenshot

Multiple injections can be defined, using the Create button, as shown in Figure A-9. For this simulation, Injection Type was set to group, Number of Particle Streams set to 200, Material set to coal-hv (which has the same density as sand), and the starting and ending points were declared as shown in Figure A-10.

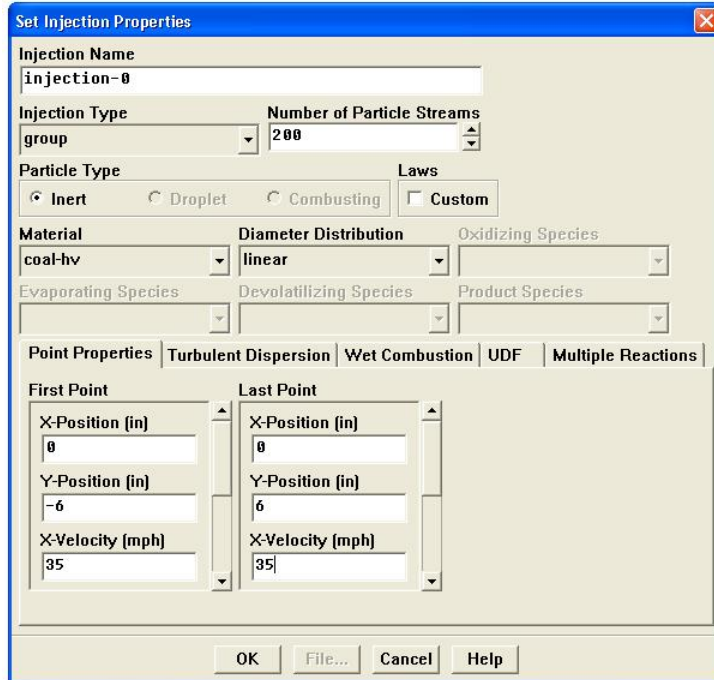


Figure A-10 Set Injection Properties screenshot

G. To release the particles into the velocity field, use: Display → Particle Tracks
→ Release From Injections

Select the injection that will be tested, and click Display, as shown in Figure A-11. The particle paths will then be displayed on the graph, and the particle entrapment in the windscreen can be seen.

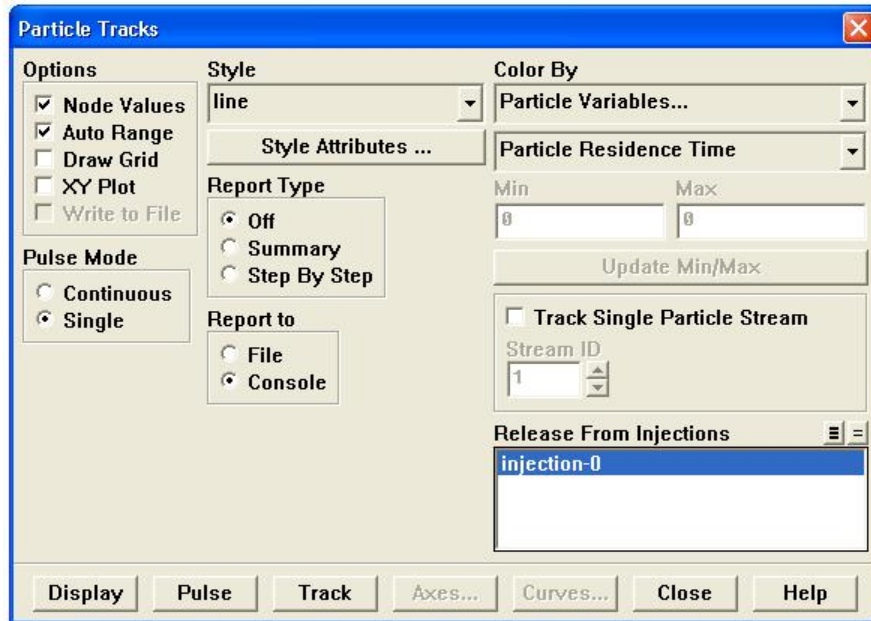


Figure A-11 Particle Tracks screenshot

MATLAB CODE

M-file for wind noise testing from DAT tape

```
%% M-file to find wind noise from 0-30, or 0-100 Hz
%% Created by: Jeff Hill
%% Updated: 11/19/2005

clear all;

% x is the upper limit for frequencies, either 31 or 101
x=31;

% Add gain, calibration, etc.
gain=10;
calibration1 = .05734;
calibration2 = .05763;
samplerate=48000;
mmm=48000;
delttime=1/samplerate;

% Run through each path
for ii=21:50

    % Each run has two windspeeds
    eval([ strcat('addpath run' num2str(ii-1) ' ') ]);
    lowwind = load('lowwind.asc','-ascii');
    highwind = load('highwind.asc','-ascii');

    % Each windspeed is cut in half
    lowwind1 = lowwind(1:96000,:);
    lowwind2 = lowwind(96001:192000,:);
    highwind1 = highwind(1:96000,:);
    highwind2 = highwind(96001:192000,:);

    % Increment frequency
    delfreq = 1/(mmm*delttime);
    incr = 0:1:mmm-1;
    freq = incr * delfreq;

    % Take FFT of each variable
    low11=1/(gain*calibration1*mmm)*fft(lowwind1(1:mmm,1));
    low12=1/(gain*calibration2*mmm)*fft(lowwind1(1:mmm,2));
```

```

high11=1/(gain*calibration1*mmm)*fft(highwind1(1:mmm,1));
high12=1/(gain*calibration2*mmm)*fft(highwind1(1:mmm,2));
low21=1/(gain*calibration1*mmm)*fft(lowwind2(1:mmm,1));
low22=1/(gain*calibration2*mmm)*fft(lowwind2(1:mmm,2));
high21=1/(gain*calibration1*mmm)*fft(highwind2(1:mmm,1));
high22=1/(gain*calibration2*mmm)*fft(highwind2(1:mmm,2));

% Find dB levels for each variable
dBlow11=20*log10(abs(low11)/.00002);
dBlow12=20*log10(abs(low12)/.00002);
dBhigh11=20*log10(abs(high11)/.00002);
dBhigh12=20*log10(abs(high12)/.00002);
dBlow21=20*log10(abs(low21)/.00002);
dBlow22=20*log10(abs(low22)/.00002);
dBhigh21=20*log10(abs(high21)/.00002);
dBhigh22=20*log10(abs(high22)/.00002);

% Send output to matrix
Output(ii,1)=mean(dBlow11(2:x)); %averagelow1
Output(ii,2)=mean(dBlow21(2:x)); %averagelow1
Output(ii,3)=max(dBlow11(2:x)); %maxlow1
Output(ii,4)=max(dBlow21(2:x)); %maxlow1
Output(ii,5)=std(dBlow11(2:x)); %standard deviation
Output(ii,6)=std(dBlow21(2:x)); %standard deviation

Output(ii,7)=mean(dBlow12(2:x)); %averagelow2
Output(ii,8)=mean(dBlow22(2:x)); %averagelow2
Output(ii,9)=max(dBlow12(2:x)); %maxlow2
Output(ii,10)=max(dBlow22(2:x)); %maxlow2
Output(ii,11)=std(dBlow12(2:x)); %stdlow2
Output(ii,12)=std(dBlow22(2:x)); %stdlow2

Output(ii,13)=mean(dBhigh11(2:x)); %averagehigh1
Output(ii,14)=mean(dBhigh21(2:x)); %averagehigh1
Output(ii,15)=max(dBhigh11(2:x)); %maxhigh1
Output(ii,16)=max(dBhigh21(2:x)); %maxhigh1
Output(ii,17)=std(dBhigh11(2:x)); %stdhigh1
Output(ii,18)=std(dBhigh21(2:x)); %stdhigh1

Output(ii,19)=mean(dBhigh12(2:x)); %averagehigh2
Output(ii,20)=mean(dBhigh22(2:x)); %averagehigh2
Output(ii,21)=max(dBhigh12(2:x)); %maxhigh2
Output(ii,22)=max(dBhigh22(2:x)); %maxhigh2
Output(ii,23)=std(dBhigh12(2:x)); %stdhigh2
Output(ii,24)=std(dBhigh22(2:x)); %stdhigh2

```

```
end
```

M-file for insertion loss from DAT tape

```
%% M-file to find amplitude peak at a given frequency
%% Created by: Jeff Hill
%% Updated: 11/12/2005

clear all;

% Load frequencies
f=[50 50 75 75 100 100 150 150 200 200 400 400 750 750 1000 1000 2000 2000
5000 5000 10000 10000];

% Declare gain, mic calibration, sample rate, etc.
gain=10;
calibration1 = .05734;
calibration2 = .05763;
samplerate=48000;
delttime=1/samplerate;

% Load time series data for each voltage (taken from DAT tape)
voltage50 = load('50.asc','-ascii');
voltage50a = load('50a.asc','-ascii');
voltage75 = load('75.asc','-ascii');
voltage75a = load('75a.asc','-ascii');
voltage100 = load('100.asc','-ascii');
voltage100a = load('100a.asc','-ascii');
voltage150 = load('150.asc','-ascii');
voltage150a = load('150a.asc','-ascii');
voltage200 = load('200.asc','-ascii');
voltage200a = load('200a.asc','-ascii');
voltage400 = load('400.asc','-ascii');
voltage400a = load('400a.asc','-ascii');
voltage750 = load('750.asc','-ascii');
voltage750a = load('750a.asc','-ascii');
voltage1000 = load('1000.asc','-ascii');
voltage1000a = load('1000a.asc','-ascii');
voltage2000 = load('2000.asc','-ascii');
voltage2000a = load('2000a.asc','-ascii');
voltage5000 = load('5000.asc','-ascii');
```

```

voltage5000a = load('5000a.asc','-ascii');
voltage10000 = load('10000.asc','-ascii');
voltage10000a = load('10000a.asc','-ascii');

% load all voltages into one matrix
voltage=[voltage50 voltage50a voltage75 voltage75a voltage100 voltage100a
voltage150 voltage150a voltage200 voltage200a voltage400 voltage400a voltage750
voltage750a voltage1000 voltage1000a voltage2000 voltage2000a voltage5000
voltage5000a voltage10000 voltage10000a];

kk=1;
for ii=1:2:size(voltage,2)

% Add calibration and gain for each voltage ii
pressure1=(voltage(:,ii)/(gain*calibration1));
pressure2=(voltage(:,ii+1)/(gain*calibration2));

% Seperate signal into three cases
for jj=1:32768

pressure1a(jj)=pressure1(jj);
pressure1b(jj)=pressure1(jj+samplerate);
pressure1c(jj)=pressure1(jj+(2*samplerate));
pressure2a(jj)=pressure2(jj);
pressure2b(jj)=pressure2(jj+samplerate);
pressure2c(jj)=pressure2(jj+(2*samplerate));
end

% Take FFT of data
Y1a=1/length(pressure1a)*fft(pressure1a);
Y1b=1/length(pressure1b)*fft(pressure1b);
Y1c=1/length(pressure1c)*fft(pressure1c);
Y2a=1/length(pressure2a)*fft(pressure2a);
Y2b=1/length(pressure2b)*fft(pressure2b);
Y2c=1/length(pressure2c)*fft(pressure2c);

delfreq = 1/(length(pressure1a)*delttime);

index = round(f(kk)/delfreq)+1;

```

```

% Add frequency incrementation
incr = 0:1:length(pressure1a)-1;
freq = incr * delfreq;

% Find dB of peak amplitude
dB1a = 20*log10(abs(Y1a)/.00002);
dB1b = 20*log10(abs(Y1b)/.00002);
dB1c = 20*log10(abs(Y1c)/.00002);
dB2a = 20*log10(abs(Y2a)/.00002);
dB2b = 20*log10(abs(Y2b)/.00002);
dB2c = 20*log10(abs(Y2c)/.00002);

% Add dB level to matrix so it carries through
dBlevel(kk,1)=dB1a(index);
dBlevel(kk,2)=dB1b(index);
dBlevel(kk,3)=dB1c(index);
dBlevel(kk,4)=dB2a(index);
dBlevel(kk,5)=dB2b(index);
dBlevel(kk,6)=dB2c(index);

% Delete everything but final value
clear pressure1 pressure1a pressure1b pressure1c Y delfreq index incr freq
dB1a;
clear pressure2 pressure2a pressure2b pressure2c dB1b dB1c dB2a dB2b
dB2c;

kk=kk+1;
end

```

M-file for wind noise testing from DataPhysics

```

%% M-file to find wind noise from f1 to f2 Hz
%% Created by: Jeff Hill
%% Updated: 3/29/2005

clear all;

% Decide frequency range
f1=1;
f2=100;

% Bring in all the data
[ freq highwindspider]=textread('ascii00026/G1, 1sv00000.txt','%f %f', -

```

```

1,'headerlines', 7);
    [freq lowwindspider]=textread('ascii00027/G1, 1sv00000.txt','%f %f', -
1,'headerlines', 7);
    [freq lowwindnothing]=textread('ascii00028/G1, 1sv00000.txt','%f %f', -
1,'headerlines', 7);
    [freq highwindnothingperp]=textread('ascii00029/G1, 1sv00000.txt','%f %f', -
1,'headerlines', 7);
    [freq highwindnothingpar]=textread('ascii00030/G1, 1sv00000.txt','%f %f', -
1,'headerlines', 7);
    [freq highwindconeperp]=textread('ascii00031/G1, 1sv00000.txt','%f %f', -
1,'headerlines', 7);
    [freq highwindconeperp]=textread('ascii00032/G1, 1sv00000.txt','%f %f', -
1,'headerlines', 7);

% Take dB of the data
dBhighspider=20*log10(highwindspider/.00002);
dBblowspider=20*log10(lowwindspider/.00002);
dBblownothing=20*log10(lowwindnothing/.00002);
dBhighnothingperp=20*log10(highwindnothingperp/.00002);
dBhighnothingpar=20*log10(highwindnothingpar/.00002);
dBhighconeperp=20*log10(highwindconeperp/.00002);
dBhighconeperp=20*log10(highwindconeperp/.00002);

% Take average
AvedBhighspider = mean(dBhighnothingperp(f1:f2)-dBhighspider(f1:f2))
AvedBlowspider = mean(dBlownothing(f1:f2)-dBblowspider(f1:f2))
AvedBhighconeperp = mean(dBhighnothingperp(f1:f2)-dBhighconeperp(f1:f2))
AvedBhighconeperp = mean(dBhighnothingpar(f1:f2)-dBhighconeperp(f1:f2))

%Plot High Windspeed for Spider
figure(1)
plot(freq,dBhighnothingperp,freq,dBhighspider)
title('Wind noise reduction in 20 MPH wind')
xlabel('Frequency (Hz)')
ylabel('SPL (dB)')
axis([f1 f2 20 90]);
legend('Nothing','Spider');

% Plot Low Windspeed for Spider
figure(2)
plot(freq,dBlownothing,freq,dBlowspider)
title('Wind noise reduction in 13 MPH wind')
xlabel('Frequency (Hz)')
ylabel('SPL (dB)')
axis([f1 f2 0 100]);
legend('Nothing','Spider');

```

```

% Plot High Windspeed for Perpendicular Cone
figure(3)
plot(freq,dBhighnothingperp,freq,dBhighconeperp)
title('Wind noise reduction for Cone windscreen (20 MPH)')
xlabel('Frequency (Hz)')
ylabel('SPL (dB)')
axis([f1 f2 40 80]);
legend('Nothing','Cone');

% Plot High Windspeed for Parrallel Cone
figure(4)
plot(freq,dBhighnothingpar,freq,dBhighconeapar)
title('Wind noise reduction for Cone windscreen (20 MPH)')
xlabel('Frequency (Hz)')
ylabel('SPL (dB)')
axis([f1 f2 0 100]);
legend('Nothing','Cone (Parrallel)');

```

M-file for insertion loss testing from DataPhysics

```

%% M-file to find wind noise from f1 to f2 Hz
%% Created by: Jeff Hill
%% Updated: 12/10/2004

clear all;

% Initialize gain, calibration, etc.
q=16384;
gain=1;
calibration1 = .05734;
calibration2 = .05763;
samplerate=25600;
mmm=16384;
delttime=1/samplerate;
x=12;

% Read in data
[time v100z]=textread('ascii00229/X1sv00000.txt','%f %f', -1,'headerlines', 7);
[time v100]=textread('ascii00229/X2sv00000.txt','%f %f', -1,'headerlines', 7);
voltage100=[v100(1:q) v100z(1:q)];
voltage100a=[v100(q+1:2*q) v100z(q+1:2*q)];

[time v200z]=textread('ascii00230/X1sv00000.txt','%f %f', -1,'headerlines', 7);

```

```

[time v200]=textread('ascii00230/X2sv00000.txt','%f %f', -1,'headerlines', 7);
voltage200=[v200(1:q) v200z(1:q)];
voltage200a=[v200(q+1:2*q) v200z(q+1:2*q)];

[time v500z]=textread('ascii00231/X1sv00000.txt','%f %f', -1,'headerlines', 7);
[time v500]=textread('ascii00231/X2sv00000.txt','%f %f', -1,'headerlines', 7);
voltage500=[v500(1:q) v500z(1:q)];
voltage500a=[v500(q+1:2*q) v500z(q+1:2*q)];

[time v1000z]=textread('ascii00232/X1sv00000.txt','%f %f', -1,'headerlines', 7);
[time v1000]=textread('ascii00232/X2sv00000.txt','%f %f', -1,'headerlines', 7);
voltage1000=[v1000(1:q) v1000z(1:q)];
voltage1000a=[v1000(q+1:2*q) v1000z(q+1:2*q)];

% Increment frequencies
delfreq = 1/(mmm*delttime);
incr = 0:1:mmm-1;
freq = incr * delfreq;

% Index the frequencies
index100 = round(100/delfreq)+1;
index200 = round(200/delfreq)+1;
index500 = round(500/delfreq)+1;
index1000 = round(1000/delfreq)+1;

% Take FFT of data
Y1Y100=1/(gain*calibration1*mmm)*fft(voltage100(1:mmm,1));
Y2Y100=1/(gain*calibration2*mmm)*fft(voltage100(1:mmm,2));
Y1Y100a=1/(gain*calibration1*mmm)*fft(voltage100a(1:mmm,1));
Y2Y100a=1/(gain*calibration2*mmm)*fft(voltage100a(1:mmm,2));

Y1Y200=1/(gain*calibration1*mmm)*fft(voltage200(1:mmm,1));
Y2Y200=1/(gain*calibration2*mmm)*fft(voltage200(1:mmm,2));
Y1Y200a=1/(gain*calibration1*mmm)*fft(voltage200a(1:mmm,1));
Y2Y200a=1/(gain*calibration2*mmm)*fft(voltage200a(1:mmm,2));

Y1Y500=1/(gain*calibration1*mmm)*fft(voltage500(1:mmm,1));
Y2Y500=1/(gain*calibration2*mmm)*fft(voltage500(1:mmm,2));
Y1Y500a=1/(gain*calibration1*mmm)*fft(voltage500a(1:mmm,1));
Y2Y500a=1/(gain*calibration2*mmm)*fft(voltage500a(1:mmm,2));

Y1Y1000=1/(gain*calibration1*mmm)*fft(voltage1000(1:mmm,1));
Y2Y1000=1/(gain*calibration2*mmm)*fft(voltage1000(1:mmm,2));
Y1Y1000a=1/(gain*calibration1*mmm)*fft(voltage1000a(1:mmm,1));
Y2Y1000a=1/(gain*calibration2*mmm)*fft(voltage1000a(1:mmm,2));

```

```

% Take dB of desired frequency
z=1;
dB(z,1)=20*log10(abs(Y1Y100(index100))/0.00002);
dB(z,2)=20*log10(abs(Y2Y100(index100))/0.00002);
dB(z+1,1)=20*log10(abs(Y1Y100a(index100))/0.00002);
dB(z+1,2)=20*log10(abs(Y2Y100a(index100))/0.00002);
z=z+2;

dB(z,1)=20*log10(abs(Y1Y200(index200))/0.00002);
dB(z,2)=20*log10(abs(Y2Y200(index200))/0.00002);
dB(z+1,1)=20*log10(abs(Y1Y200a(index200))/0.00002);
dB(z+1,2)=20*log10(abs(Y2Y200a(index200))/0.00002);
z=z+2;

dB(z,1)=20*log10(abs(Y1Y500(index500))/0.00002);
dB(z,2)=20*log10(abs(Y2Y500(index500))/0.00002);
dB(z+1,1)=20*log10(abs(Y1Y500a(index500))/0.00002);
dB(z+1,2)=20*log10(abs(Y2Y500a(index500))/0.00002);
z=z+2;

dB(z,1)=20*log10(abs(Y1Y1000(index1000))/0.00002);
dB(z,2)=20*log10(abs(Y2Y1000(index1000))/0.00002);
dB(z+1,1)=20*log10(abs(Y1Y1000a(index1000))/0.00002);
dB(z+1,2)=20*log10(abs(Y2Y1000a(index1000))/0.00002);

```

M-file for phase shift testing from DataPhysics

```

%% M-file to find wind noise from f1 to f2 Hz
%% Created by: Jeff Hill
%% Updated: 3/07/2005

clear all;

% Initialize calibration, etc.
q=16384;
gain=1;
calibration = .05;
mmm=8192;
x=12;

% Read in time series data for each microphone for each run
[time N0(:,1)]=textread('ascii00015/X1sv00000.txt','%f %f', -1,'headerlines', 7);

```



```

% Increment frequency, etc
delttime=(time(3)-time(2));
samplerate = 1/delttime;
delfreq = 1/(mmm*delttime);
incr = 0:1:mmm-1;
freq = incr * delfreq;
index500 = round(500/delfreq)+1;

% Take FFT of data
N11N0=1/(gain*calibration*mmm)*fft(N0(1:mmm,1));
N12N0=1/(gain*calibration*mmm)*fft(N0(1:mmm,2));
N13N0=1/(gain*calibration*mmm)*fft(N0(1:mmm,3));
N14N0=1/(gain*calibration*mmm)*fft(N0(1:mmm,4));
N15N0=1/(gain*calibration*mmm)*fft(N0(1:mmm,5));

N11N10=1/(gain*calibration*mmm)*fft(N10(1:mmm,1));
N12N10=1/(gain*calibration*mmm)*fft(N10(1:mmm,2));
N13N10=1/(gain*calibration*mmm)*fft(N10(1:mmm,3));
N14N10=1/(gain*calibration*mmm)*fft(N10(1:mmm,4));
N15N10=1/(gain*calibration*mmm)*fft(N10(1:mmm,5));

N11N20=1/(gain*calibration*mmm)*fft(N20(1:mmm,1));
N12N20=1/(gain*calibration*mmm)*fft(N20(1:mmm,2));
N13N20=1/(gain*calibration*mmm)*fft(N20(1:mmm,3));
N14N20=1/(gain*calibration*mmm)*fft(N20(1:mmm,4));
N15N20=1/(gain*calibration*mmm)*fft(N20(1:mmm,5));

N11N30=1/(gain*calibration*mmm)*fft(N30(1:mmm,1));
N12N30=1/(gain*calibration*mmm)*fft(N30(1:mmm,2));
N13N30=1/(gain*calibration*mmm)*fft(N30(1:mmm,3));
N14N30=1/(gain*calibration*mmm)*fft(N30(1:mmm,4));
N15N30=1/(gain*calibration*mmm)*fft(N30(1:mmm,5));

N11N40=1/(gain*calibration*mmm)*fft(N40(1:mmm,1));
N12N40=1/(gain*calibration*mmm)*fft(N40(1:mmm,2));
N13N40=1/(gain*calibration*mmm)*fft(N40(1:mmm,3));
N14N40=1/(gain*calibration*mmm)*fft(N40(1:mmm,4));
N15N40=1/(gain*calibration*mmm)*fft(N40(1:mmm,5));

N11N50=1/(gain*calibration*mmm)*fft(N50(1:mmm,1));
N12N50=1/(gain*calibration*mmm)*fft(N50(1:mmm,2));
N13N50=1/(gain*calibration*mmm)*fft(N50(1:mmm,3));
N14N50=1/(gain*calibration*mmm)*fft(N50(1:mmm,4));
N15N50=1/(gain*calibration*mmm)*fft(N50(1:mmm,5));

```

```

N11N60=1/(gain*calibration*mmm)*fft(N60(1:mmm,1));
N12N60=1/(gain*calibration*mmm)*fft(N60(1:mmm,2));
N13N60=1/(gain*calibration*mmm)*fft(N60(1:mmm,3));
N14N60=1/(gain*calibration*mmm)*fft(N60(1:mmm,4));
N15N60=1/(gain*calibration*mmm)*fft(N60(1:mmm,5));

```

```

N11N70=1/(gain*calibration*mmm)*fft(N70(1:mmm,1));
N12N70=1/(gain*calibration*mmm)*fft(N70(1:mmm,2));
N13N70=1/(gain*calibration*mmm)*fft(N70(1:mmm,3));
N14N70=1/(gain*calibration*mmm)*fft(N70(1:mmm,4));
N15N70=1/(gain*calibration*mmm)*fft(N70(1:mmm,5));

```

```

% Find phase of data

```

```

phase(1,1)=0;
phase(1,2)=atan2(imag(N11N0(index500)),real(N11N0(index500)));
phase(1,3)=atan2(imag(N12N0(index500)),real(N12N0(index500)));
phase(1,4)=atan2(imag(N13N0(index500)),real(N13N0(index500)));
phase(1,5)=atan2(imag(N14N0(index500)),real(N14N0(index500)));
phase(1,6)=atan2(imag(N15N0(index500)),real(N15N0(index500)));

```

```

phase(2,1)=10;
phase(2,2)=atan2(imag(N11N10(index500)),real(N11N10(index500)));
phase(2,3)=atan2(imag(N12N10(index500)),real(N12N10(index500)));
phase(2,4)=atan2(imag(N13N10(index500)),real(N13N10(index500)));
phase(2,5)=atan2(imag(N14N10(index500)),real(N14N10(index500)));
phase(2,6)=atan2(imag(N15N10(index500)),real(N15N10(index500)));

```

```

phase(3,1)=20;
phase(3,2)=atan2(imag(N11N20(index500)),real(N11N20(index500)));
phase(3,3)=atan2(imag(N12N20(index500)),real(N12N20(index500)));
phase(3,4)=atan2(imag(N13N20(index500)),real(N13N20(index500)));
phase(3,5)=atan2(imag(N14N20(index500)),real(N14N20(index500)));
phase(3,6)=atan2(imag(N15N20(index500)),real(N15N20(index500)));

```

```

phase(4,1)=30;
phase(4,2)=atan2(imag(N11N30(index500)),real(N11N30(index500)));
phase(4,3)=atan2(imag(N12N30(index500)),real(N12N30(index500)));
phase(4,4)=atan2(imag(N13N30(index500)),real(N13N30(index500)));
phase(4,5)=atan2(imag(N14N30(index500)),real(N14N30(index500)));
phase(4,6)=atan2(imag(N15N30(index500)),real(N15N30(index500)));

```

```

phase(5,1)=40;
phase(5,2)=atan2(imag(N11N40(index500)),real(N11N40(index500)));
phase(5,3)=atan2(imag(N12N40(index500)),real(N12N40(index500)));
phase(5,4)=atan2(imag(N13N40(index500)),real(N13N40(index500)));

```

```

phase(5,5)=atan2(imag(N14N40(index500)),real(N14N40(index500)));
phase(5,6)=atan2(imag(N15N40(index500)),real(N15N40(index500)));

phase(6,1)=50;
phase(6,2)=atan2(imag(N11N50(index500)),real(N11N50(index500)));
phase(6,3)=atan2(imag(N12N50(index500)),real(N12N50(index500)));
phase(6,4)=atan2(imag(N13N50(index500)),real(N13N50(index500)));
phase(6,5)=atan2(imag(N14N50(index500)),real(N14N50(index500)));
phase(6,6)=atan2(imag(N15N50(index500)),real(N15N50(index500)));

phase(7,1)=60;
phase(7,2)=atan2(imag(N11N60(index500)),real(N11N60(index500)));
phase(7,3)=atan2(imag(N12N60(index500)),real(N12N60(index500)));
phase(7,4)=atan2(imag(N13N60(index500)),real(N13N60(index500)));
phase(7,5)=atan2(imag(N14N60(index500)),real(N14N60(index500)));
phase(7,6)=atan2(imag(N15N60(index500)),real(N15N60(index500)));

phase(8,1)=70;
phase(8,2)=atan2(imag(N11N70(index500)),real(N11N70(index500)));
phase(8,3)=atan2(imag(N12N70(index500)),real(N12N70(index500)));
phase(8,4)=atan2(imag(N13N70(index500)),real(N13N70(index500)));
phase(8,5)=atan2(imag(N14N70(index500)),real(N14N70(index500)));
phase(8,6)=atan2(imag(N15N70(index500)),real(N15N70(index500)));

%Locate phase in same quadrant for each data point
for ii=2:6
    for iii = 1:3
        if phase(iii,ii)< -pi
            phase(iii,ii)=phase(iii,ii)+2*pi;
        end

        if phase(iii,ii)> pi
            phase(iii,ii)=phase(iii,ii)-2*pi;
        end
    end
end
end

phase = phase';

```